

**EFFECT OF TRANSVERSE ISOTROPY ON
MECHANICAL PROPERTIES OF MAHA
SARAKHAM SALT**



**A Thesis Submitted in Partial Fulfillment of the Requirements for
the Degree of Master of Engineering in Civil, Transportation and**

Geo-Resources Engineering

Suranaree University of Technology

Academic Year 2020

ผลกระทบของทรานเวอร์สไอโซโทรปีต่อสมบัติเชิงกล
ของเกลือหินชุดมหาสารคาม



นายณัฐพล สุขเจริญ

วิทยานิพนธ์นี้เป็นส่วนหนึ่งของการศึกษาตามหลักสูตรปริญญาวิศวกรรมศาสตรมหาบัณฑิต
สาขาวิชาวิศวกรรมโยธา ขนส่ง และทรัพยากรธรณี
มหาวิทยาลัยเทคโนโลยีสุรนารี
ปีการศึกษา 2563

**EFFECT OF TRANSVERSE ISOTROPY ON MECHANICAL
PROPERTIES OF MAHA SARAKHAM SALT**

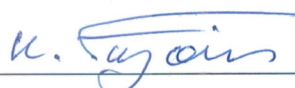
Suranaree University of Technology has approved this thesis submitted in partial fulfillment of the requirements for a Master's Degree.

Thesis Examining Committee




(Assoc. Prof. Dr. Pornkasem Jongpradist)

Chairperson




(Prof. Dr. Kittitep Fuenkajorn)

Member (Thesis Advisor)



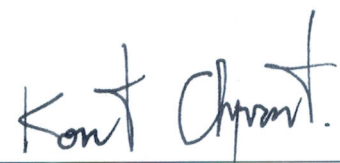
(Asst. Prof. Dr. Akkhapun Wannakomol)

Member



(Dr. Thanittha Thongrapha)

Member



(Assoc. Prof. Ft. Lt. Dr. Kontorn Chamnirasart)

Vice Rector for Academic Affairs
and Internationalization



(Assoc. Prof. Dr. Pornsiri Jongkol)

Dean of Institute of Engineering

ณัฐพล สุขเจริญ : ผลกระทบของทรานเวอร์สไอโซโทรปีต่อสมบัติเชิงกลของเกลือหินชุด
มหาสารคาม (EFFECT OF TRANSVERSE ISOTROPY ON MECHANICAL
PROPERTIES OF MAHA SARAKHAM SALT) อาจารย์ที่ปรึกษา : ศาสตราจารย์ ดร.กิตติ
เทพ เพื่อขจร, 64 หน้า.

การทดสอบแรงกดแบบแกนเดียวและแบบสามแกนได้ถูกดำเนินการบนตัวอย่างเกลือหิน
ทรงปริซึมที่มีขนาด $54 \times 54 \times 108$ ลูกบาศก์มิลลิเมตร เพื่อหาผลกระทบของทรานเวอร์ส
ไอโซโทรปีต่อกำลังรับแรงและการเปลี่ยนแปลงรูปร่างของตัวอย่างเกลือหินที่มีการวางตัวของ
ระนาบชั้นหินแตกต่างกันภายใต้ความดันล้อมรอบสูงถึง 15 เมกะปาสกาล ผลที่ได้ระบุว่ากำลังรับ
แรงกดมีค่าสูงสุดเมื่อแรงกดมีทิศทางตั้งฉากกับระนาบชั้นหิน และกำลังรับแรงต่ำสุดจะเกิดขึ้นเมื่อ
แรงตั้งฉากกับระนาบชั้นหินทำมุม 60 องศากับทิศทางการให้แรง โดยเฉพาะอย่างยิ่งภายใต้ความดัน
ล้อมรอบต่ำ ค่าสัมประสิทธิ์ความยืดหยุ่นและอัตราส่วนปัวซองส์ได้ถูกคำนวณบนพื้นฐานของ
สมการทรานเวอร์สไอโซโทรปีที่น่าเสนอโดย Amadei ผลกระทบของทรานเวอร์ส
ไอโซโทรปีลดลงเมื่อเกลือหินอยู่ภายใต้แรงดันล้อมรอบที่สูงขึ้น โดยเกลือหินมีแนวโน้มที่จะ
กลายเป็นวัสดุไอโซโทรปี เนื่องจากตัวอย่างเกลือหินมีคุณสมบัติในการเชื่อมประสานตัวเองภายใต้
ความดันล้อมรอบ ส่งผลให้มีพฤติกรรมแบบแอนไอโซโทรปีลดลง การค้นพบนี้สามารถใช้เพื่อ
ประเมินกำลังรับแรงและการเปลี่ยนแปลงรูปร่างของเสาเกลือหินและผนังด้านข้างของช่องเหมืองที่
มีการวางตัวของระนาบชั้นหินแตกต่างกัน

สาขาวิชา เทคโนโลยีธรณี
ปีการศึกษา 2563

ลายมือชื่อนักศึกษา ณัฐพล สุขเจริญ
ลายมือชื่ออาจารย์ที่ปรึกษา ก. เทพ

NATTAPON SUKJAROEN : EFFECT OF TRANSVERSE ISOTROPY ON
MECHANICAL PROPERTIES OF MAHA SARAKHAM SALT.

THESIS ADVISOR : PROF. KITTITEP FUENKAJORN, Ph.D., P.E., 64 PP.

ANISOTROPY/BEDDED SALT/ELASTICITY/STRENGTH

Uniaxial and triaxial compression tests have been performed on prismatic salt specimens having nominal dimensions of $54 \times 54 \times 108 \text{ mm}^3$ to determine the transversely isotropic effect on strength and deformation of rock salt specimens with different bedding plane orientations under confining pressures up to 15 MPa. The results indicate that the compressive strength is maximum when loading is perpendicular to the bedding (anisotropic) planes. The minimum strength occurs when normal to the bedding planes makes an angle of 60 degrees with the loading direction, especially under lower confining pressures. The elastic moduli and Poisson's ratios are calculated based on the transversely isotropic solutions proposed by Amadei. The effect of transversely isotropy decreases when salt is subjected to higher confining pressures where the salt tends to behave as an isotropic material. This is probably because the salt specimens have ability of self-healing under confinement, and hence decreases their anisotropic behavior. The findings obtained here can be used to assess the strengths and deformability of salt pillars and sidewall of opening that contain various orientations of bedding planes.

School of Geotechnology

Academic Year 2020

Student's Signature 

Advisor's Signature 

ACKNOWLEDGMENTS

I wish to acknowledge the funding supported by Suranaree University of Technology (SUT).

I would like to express my sincere thanks to Prof. Dr. Kittitep Fuenkajorn for his valuable guidance and efficient supervision. I appreciate his strong support, encouragement, suggestions and comments during the research period. My heartiness thanks to Assoc. Prof. Dr. Pornkasem Jongpradist, Asst. Prof. Dr. Akkhapun Wannakomol and Dr. Thanittha Thonggrapha for their constructive advice, valuable suggestions and comments on my research works as thesis committee members. Grateful thanks are given to all staffs of Geomechanics Research Unit, Institute of Engineering who supported my work.

Finally, I would like to thank beloved parents for their love, support and encouragement.

Nattapon Sukjaroen

TABLE OF CONTENTS

	Page
ABSTRACT (THAI).....	I
ABSTRACT (ENGLISH).....	II
ACKNOWLEDGEMENTS.....	III
TABLE OF CONTENTS.....	IV
LIST OF TABLES.....	VII
LIST OF FIGURES.....	VIII
SYMBOLS AND ABBREVIATIONS.....	XII
CHAPTER	
I INTRODUCTION.....	1
1.1 Background and rationale.....	1
1.2 Research objectives.....	1
1.3 Scope and limitations.....	1
1.4 Research methodology.....	1
1.4.1 Literature review.....	2
1.4.2 Salt specimen preparation.....	3
1.4.3 Uniaxial and triaxial compression tests.....	4
1.4.4 Development of strength criterion.....	4
1.4.5 Determination of elastic parameters.....	4
1.4.6 Applications to salt pillar analysis.....	4

TABLE OF CONTENTS (Continued)

	Page
1.4.7 Discussions and conclusions.....	4
1.4.8 Thesis writing.....	5
1.5 Thesis contents.....	5
II LITERATURE REVIEW.....	6
2.1 Mechanical properties of Maha Sarakham.....	6
2.2 Effect of transverse isotropy on rock strength.....	8
2.3 Effect of transverse isotropy on elastic properties of rocks.....	11
2.4 Analysis of transversely isotropic effect on elastic property of materials.....	13
III SAMPLE PREPARATION.....	16
3.1 Introduction.....	16
3.2 Sample preparation.....	16
3.3 X-ray diffraction analysis.....	19
IV LABORATORY TESTING.....	20
4.1 Introduction.....	20
4.2 Test methods.....	20
4.3 Test results.....	23
V STRENGTH CRITERIA.....	32
5.1 Introduction.....	32

TABLE OF CONTENTS (Continued)

	Page
5.2 Hoek and Brown criterion.....	32
5.3 Coulomb criterion.....	35
5.4 Strength criterion based on strain energy density.....	38
5.5 Discussions of the test results.....	39
VI TRANSVERSELY ISOTROPIC EFFECT ON	
SALT ELASTICITY	44
6.1 Introduction.....	44
6.2 Degrees of rock anisotropy.....	44
6.3 Transverse isotropic parameters.....	46
6.3.1 Apparent elastic modulus.....	47
6.3.2 Apparent Poisson's ratio.....	47
VII SALT PILLAR STABILITY ANALYSIS	50
7.1 Introduction.....	50
7.2 Pillar stress.....	50
VIII DISCUSSIONS AND CONCLUSIONS	55
7.1 Discussions.....	55
7.2 Conclusions.....	56
7.3 Recommendations for future studies.....	57
REFERENCES.....	59
BIOGRAPHY.....	64

LIST OF TABLES

Table	Page
3.1 Salt specimens prepared for uniaxial and triaxial compression tests.....	18
3.2 Results of X-ray diffraction analysis.....	19
4.1 Compression test results.....	24
5.1 Orientation angles and their constants calibrated from compression test data.....	33
5.2 Friction angles and cohesions for difference orientation angles from the test data.....	36
5.3 Strain energy of each specimen.....	39
6.1 Results of E/E' ratios.....	45
6.2 Apparent elastic properties determined on rock salt using uniaxial and triaxial compression test results.....	47
7.1 Depth and factors of safety at different orientation angles.....	54

LIST OF FIGURES

Figure	Page
1.1 Research methodology.....	3
2.1 Result of Colak and Unlu (2004).....	10
2.2 Strength results of Goshashi et al. (2006).....	10
2.3 Strengths under different angles (Goshashi et al., 2006).....	11
2.4 Comparison of Goshashi et al. (2006).....	11
2.5 Results of Miller et al. (2013).....	12
2.6 Results of Hu et al. (2017).....	13
2.7 Examples of Amadei calculations.....	15
2.8 Young's modulus predicted by Amadei (1996).....	15
3.1 Location of Thai Kali Co., Ltd. in Khorat salt basin and typical geologic sequence of Maha Sarakham formation at mine site.....	17
3.2 Examples of specimens prepared for uniaxial compression and triaxial testing.....	19
4.1 Polyaxial load frame employed in uniaxial and triaxial testing (Fuenkajorn et al., 2012).....	21
4.2 Loading directions with respect to bedding planes (a). Elastic parameters for transversely isotropic conditions (b).....	22
4.3 Some post-test specimens of uniaxial and triaxial compression test. White lines indicate induced fractures.....	25

LIST OF FIGURES (Continued)

Figure	Page
4.4	Stress-strain curves from compression tests on salt specimens with $\beta = 0^\circ$ shows notations used in stress-strain diagrams.....26
4.5	Stress-strain curves from compression tests on salt specimens with $\beta \approx 25^\circ$ shows notations used in stress-strain diagrams.....27
4.6	Stress-strain curves from compression tests on salt specimens with $\beta \approx 45^\circ$ shows notations used in stress-strain diagrams.....28
4.7	Stress-strain curves from compression tests on salt specimens with $\beta \approx 60^\circ$ shows notations used in stress-strain diagrams.....29
4.8	Stress-strain curves from compression tests on salt specimens with $\beta = 90^\circ$ shows notations used in stress-strain diagrams.....30
4.9	Compressive strengths as a function of β for different confining pressures (σ_3).....31
4.10	Elastic moduli as a function of β for different confining pressures (σ_3).....31
5.1	Hoek–Brown criterion of salt specimens with different bedding plane angles.....33
5.2	Hoek-Brown parameter m (a) and calculated uniaxial compressive strength σ_c (b) as a function of β34
5.3	Uniaxial compressive strength (σ_c) as a function of calculated strength (σ_c').....35

LIST OF FIGURES (Continued)

Figure	Page
5.4	Maximum principal stress (σ_1) as a function of confining stress (σ_3) at failure for various orientation angles.....
	37
5.5	Cohesion, c (a) and internal friction angel, ϕ (b) as a function as of β
	38
5.6	Distortional strain energy (W_d) at at failure as a function mean stress (σ_m).....
	40
5.7	Mohr's circles form triaxial compressive strength tests on salt specimens with $\beta = 0^\circ$ in forms of Coulomb and Hoek–Brown criteria.....
	41
5.8	Mohr's circles form triaxial compressive strength tests on salt specimens with $\beta = 25^\circ$ in forms of Coulomb and Hoek–Brown criteria.....
	42
5.9	Mohr's circles form triaxial compressive strength tests on salt specimens with $\beta = 45^\circ$ in forms of Coulomb and Hoek–Brown criteria.....
	42
5.10	Mohr's circles form triaxial compressive strength tests on salt specimens with $\beta = 60^\circ$ in forms of Coulomb and Hoek–Brown criteria.....
	43

LIST OF FIGURES (Continued)

Figure	Page	
5.11	Mohr's circles from triaxial compressive strength tests on salt specimens with $\beta = 90^\circ$ in forms of Coulomb and Hoek–Brown criteria.....	43
6.1	Variation of E/E' ratios as a function of confining pressure.....	45
6.2	Variation of apparent elastic modulus (E_y) under different β angles. Lines are the calculated E_y . Data points are test results.....	48
6.3	Variation of apparent Poisson's ratio ν_{yx} (a) and ν_{yz} (b) under different β angles. Lines are the calculated apparent Poisson's ratio. Data points are test results.....	49
7.1	Factors of safety as a function of extraction ratio for five mine depths with $\beta = 0^\circ$. Solid line indicate factors of safety equal to 1.....	51
7.2	Factors of safety as a function of extraction ratio for five mine depths with $\beta = 25^\circ$. Solid line indicate factors of safety equal to 1.....	52
7.3	Factors of safety as a function of extraction ratio for five mine depths with $\beta = 45^\circ$. Solid line indicate factors of safety equal to 1.....	52
7.4	Factors of safety as a function of extraction ratio for five mine depths with $\beta = 60^\circ$. Solid line indicate factors of safety equal to 1.....	53
7.5	Factors of safety as a function of extraction ratio for five mine depths with $\beta = 90^\circ$. Solid line indicate factors of safety equal to 1.....	53

SYMBOLS AND ABBREVIATIONS

ϕ	=	Friction angle
ρ	=	In-situ stress gradient of overburden
ε	=	Strain
ν'	=	Poisson's ratio variable
ε_1	=	Major principal strain
$\nu_{1,3O}$	=	Poisson's ratio between major principal axis and the direction is normal to the strike of beds
$\nu_{1,3P}$	=	Poisson's ratio between major principal axis and the direction is parallel to the strike of beds
ε_{3O}	=	Minor principal strain measured normal to the strike of bedding planes
ε_{3P}	=	Minor principal strain measured parallel to the strike of bedding planes
$\nu_{3P,3O}$	=	Poisson's ratio between directions that are parallel and normal to strike of beds
γ_{oct}	=	Octahedral shear strain
τ_{oct}	=	Octahedral shear stress
ν_{yx}	=	Apparent Poisson's ratios
ν_{yz}	=	Apparent Poisson's ratios
G'	=	Apparent shear modulus

SYMBOLS AND ABBREVIATIONS (Continued)

σ_1	=	Major principal stress
σ_3	=	Confining pressure
σ_{3O}	=	The minor principal stresses is normal to the strike of bedding planes
σ_{3P}	=	The minor principal stresses is parallel to the strike of bedding planes
σ_c	=	Uniaxial compressive strength
σ_m	=	Mean stress
σ_n	=	Normal stress
σ_P	=	Pillar stress
σ_R	=	Stress rates
β	=	Bedding plane angles
c	=	Cohesion
e	=	Extraction ratios
E	=	Minimum elastic moduli in direction normal to the plane of transverse isotropy
E_1	=	The elastic moduli along major principal (axial) direction
E_{3O}	=	The elastic moduli along the two minor principal axes that is normal to bedding planes
E_{3P}	=	The elastic moduli along the two minor principal axes that is parallel to bedding planes

SYMBOLS AND ABBREVIATIONS (Continued)

E_y	=	Apparent elastic modulus
FS	=	The factor of safety
G'	=	Apparent shear modulus
H	=	The mine depth
K	=	Empirical parameters
k_β	=	Parameter describing the anisotropy effect
m	=	Material constants
s	=	Material constants
W_d	=	Distortional strain energy

CHAPTER I

INTRODUCTION

1.1 Background and Rationale

Several aspects of the mechanical properties of Maha Sarakham salt have been investigated for the past decade. Most laboratory testing and analyses have been conducted on the salt specimens with bedding planes normal to the core axis (major principal stress direction). A primary concern arises when one of the service mine panels (of Thai Kali Co., Ltd.) showing the support pillars and sidewall of the openings intersecting flanks of a salt fold. As a result, many pillars contain salt beds that are in vertical and nearly vertical. A question arises as how the effect of transverse isotropy of the salt affects the strengths and deformability of the supported pillars and sidewalls.

1.2 Research Objective

The objective of this study is to determine the effects of transverse isotropy on the compressive strength and elastic properties of Maha Sarakham salt. The tasks involve performing uniaxial and triaxial compression tests on rock salt, developing a strength criterion that can incorporate the transversely isotropic effect, and calculating the elastic moduli and Poisson's ratios of rock salt under various bedding orientations based on Amadei's solutions.

1.3 Scope and Limitations

The scope and limitations of the research include as follows.

- 1) Laboratory testing is conducted on rock salt specimens from Maha Sarakham formation.
- 2) Triaxial compression tests are performed with confining pressures up to 15 MPa.
- 3) The salt specimens are prepared to have different bedding plane orientations with respect to the applied loading direction.
- 4) Up to 30 samples are tested, with the nominal dimensions of $54 \times 54 \times 108$ mm³.
- 5) All tests are conducted under ambient temperature.
- 6) The research findings are published in conference paper or journal.

1.4 Research Methodology

The research methodology shown in Figure 1.1 comprises 8 steps; including literature review, salt specimen preparation, uniaxial and triaxial compression tests, development of strength criterion, determination of elastic parameters, applications to salt pillar analysis, discussions and conclusions, and thesis writing.

1.4.1 Literature Reviews

Literature review will be carried out to study researches on mechanical properties of Maha Sarakham salt, effect of transverse isotropy on rock strength, effect of transverse isotropy on elastic properties of rocks, and analysis of transversely isotropic effect on elastic property of materials. The sources of information are from journals, technical reports and conference papers.

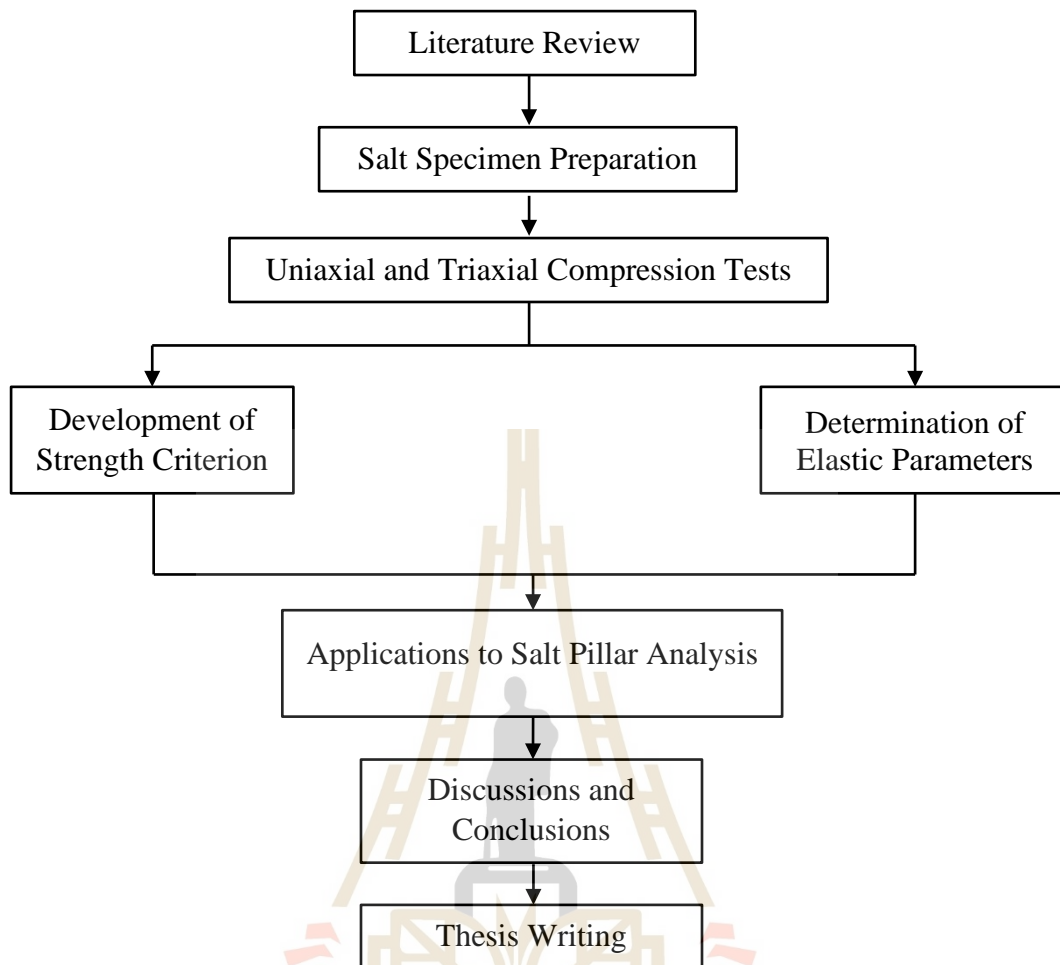


Figure 1.1 Research methodology.

1.4.2 Salt Specimen Preparation

Rock samples used here have been obtained from underground openings of Thai Kali Co., Ltd. They belong to the Lower Salt member of the Maha Sarakham formation. Sample preparation will be carried out in the laboratory at Suranaree University of Technology. The specimens are prepared to obtain rectangular blocks with nominal dimensions of $54 \times 54 \times 108 \text{ mm}^3$ for different bedding plane orientations with respect to the applied loading direction.

1.4.3 Uniaxial and Triaxial Compression Tests

A polyaxial load frame (Walsri et al., 2009) is employed to apply constant confining pressures from 0 to 15 MPa. Neoprene sheets are inserted to minimize the friction at all interfaces between the loading platens and the rock surface. The axial stress is increased until failure occurs. The confining pressure is maintained constant. The digital displacement gages are installed to measure the axial and lateral deformations. The load at failure and failure modes are recorded. They are used to calculate the strength and deformation modulus of the specimen.

1.4.4 Development of Strength Criterion

The strength result obtained from uniaxial and triaxial compression testing are used to develop failure criterion. The criterion will incorporate the effect of transverse isotropy caused by various orientations of bedding planes.

1.4.5 Determination of Elastic Parameters

The Amadei (1996) solutions are applied to evaluate the elastic moduli and Poisson's ratios of the salt specimens under various orientations of bedding planes.

1.4.6 Applications to Salt Pillar Analysis

The research findings in terms of the strength criterion of Maha Sarakham salt is used to analyze the mechanical stability of salt pillars that contain different orientations of bedding planes.

1.4.7 Discussions and Conclusions

Discussions are made to describe the reliability and adequacy of the test data. Comparison of the results obtained here with those obtained elsewhere is made in terms of similarity and discrepancy. Explanations on these issues are offered. Conclusions from the research study will be drawn.

1.4.8 Thesis Writing

All research activities, methods, and results are documented and compiled in the thesis. The research findings in the forms of strength criterion and deformability equations can be used to determine the mechanical stability and deformation of supported salt pillars that contain various orientations of bedding planes in the salt and potash mines. The findings will be published in the conference proceedings or journals.

1.5 Thesis Contents

Chapter I describes the background of problems and significance of the study. The research objectives, methodology, scope and limitations are identified. **Chapter II** summarizes the results of the literature review. **Chapter III** describes the sample preparations. **Chapter IV** describes the laboratory testing. **Chapter V** presents strength criteria. **Chapter VI** describes the transversely isotropic effect on salt elasticity. **Chapter VII** describes the salt pillar stability analysis. **Chapter VIII** discusses and concludes the research results and provides recommendations for future research studies.

CHAPTER II

LITERATURE REVIEW

This chapter describes research results on the mechanical behavior of Maha Sarakham salt that have been conducted by several investigators.

2.1 Mechanical Properties of Maha Sarakham

Samsri et al. (2010) determine effect of intermediate principal stress on creep of Maha Sarakham salt. The results indicate that the salt stiffness does not depend on the intermediate principal stress (σ_2), but it increases with shear stress. Under the same deviatoric stress, the creep parameters increase with σ_2 from the triaxial compression to the triaxial extension conditions.

The intrinsic variability of Maha Sarakham salt is examined by Fuenkajorn et al. (2011). The compressive strength linearly increases with anhydrite inclusions. The anhydrite inclusion also increases salt elasticity from 22 GPa to 36 GPa. Tensile strengths also increase with anhydrite inclusion, particularly when the content is greater than 60% by weight.

The strain energy density criterion is used by Sriapai et al. (2012) to predict the salt strength and deformability under elevated temperatures. The test results show that distortional strain energy increases with the mean strain energy. The increasing rates are the same for all temperatures.

Empirical strength criteria are used by Fuenkajorn et al. (2012) to predict the salt strength. Compression tests are performed to assess the effect of loading rate on the

strength and deformability of salt. The elastic parameters are independent of the confinement. The strains at failure reduce with increasing loading rate. Shear strain energy at dilation and at failure from different loading rates varies with mean normal stress.

The loading rate and temperature effects on tensile strength and deformation of salt under temperatures from 273 to 375 K are examined by Wisetsaen et al. (2015). The tensile strength increases with loading rate, and reduces when the temperatures are increased.

Chobsranoi and Fuenkajorn (2016) identify experimentally the effects of loading rate on tensile strength of salt under various carnallite contents. The creep tensile strengths are determined with carnallite contents from 0 to 95%. The tensile strengths decrease with increasing the carnallite contents. The strength however increases with the stress rates (σ_R) decrease.

Archeeploha et al. (2017) determine effects of intermediate principal stress (σ_2) on creep of salt. The creep parameters significantly increase with σ_2 . It was concluded that the conventional creep test results may overestimate the actual closure of cylindrical and spherical caverns by as much as 15% and 35%.

Luangthip et al. (2017) study the influence of carnallite on strength, elasticity, and creep of Maha Sarakham salt. The compressive and tensile strengths and elastic moduli decrease with increasing carnallite. Carnallite can increase dilation of salt specimens. The effect of carnallite decreases when confining pressures increase. The elastic moduli decrease with increasing carnallite. Pure halite behaves as the Burgers material while pure carnallite behaves as the Maxwell material.

Junthong et al. (2019) determine the creep strengths of salt mine pillars. A

higher strain rate applied leads to a higher stiffness of salt. Poisson's ratios also decrease when strain rates increase.

Artkhonghan et al. (2018) study the stress paths effect on strengths of Maha Sarakham salt. Under constant σ_m , the salt fails under low stress than when it is under constant σ_3 . The modified Wiebols and Cook and Mogi criteria derived from constant σ_3 test results can estimate salt strength under constant σ_m .

Phatthaisong et al. (2018) assess the thermal and rate effects on mechanical properties of salt. The salt strength and stiffness increase when loading rate increases. The decrease of the salt strength as the temperature increases indicates that the thermal energy can weaken the salt and makes it more plastic. The salt, then, fail at lower stress and lower stiffness.

2.2 Effect of Transverse Isotropy on Rock Strength

McLamore et al. (1967) determine the compressive strengths of three anisotropic rocks. The plane of anisotropy is from 0° to 90° with respect to loading axis. The anisotropic rocks fail and deform by shear along the bedding plane.

Colak and Unlu (2004) investigate the effect of joint orientation on the strength of sandstone, siltstone and claystone. The samples show orientations (β) at 0, 30, 45, 60 and 90° . Values of $m_{i(\beta)}$ of Hoek-Brown criterion vary with orientation angle. A suitable function that can used to define the normalized value of $m_{i(\beta)}$ is obtained:

$$\frac{m_{i(\beta)}}{m_{i(90)}} = 1 - A \exp \left[- \left(\frac{\beta - B}{C + D\beta} \right)^4 \right] \quad (2.1)$$

where $m_{i(90)}$ is reference value of m_i , B is value of β at which $m_{i(\beta)}$ is minimum, and A,

C and D are statistical parameters. Figure 2.1 shows the curves of the above equation.

From Equation (2.1), the parameter $m_i(\beta)$ can be further defined as:

$$\sigma_{1(\beta)}/\sigma_{ci(\beta)} = \sigma_3/\sigma_{ci(\beta)} + (m_i(\beta)\sigma_3/\sigma_{ci(\beta)} + 1)^{0.5} \quad (2.2)$$

Goshtasbi et al. (2006) propose the criterion for predicting the anisotropic strength of rocks. Figure 2.2 shows the compressive strength as a function of orientation

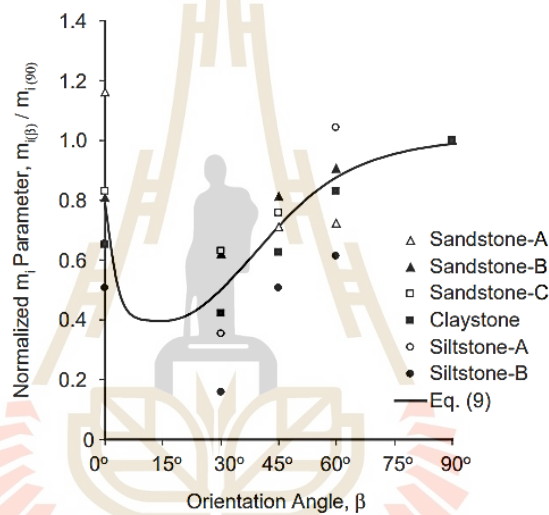


Figure 2.1 Result of Colak and Unlu (2004).

angles. The slate has a U-shaped anisotropy. Figure 2.3 shows the strength as a function of orientation angles and confining pressures. The maximum and minimum strengths are obtained at $\beta = 90^\circ$ and 30° . Liao and Hsieh (Liao and Hsieh, 1999) and Ramamurthy criteria (Ramamurthy, 1993) also conclude that both criteria can well fit the test results.

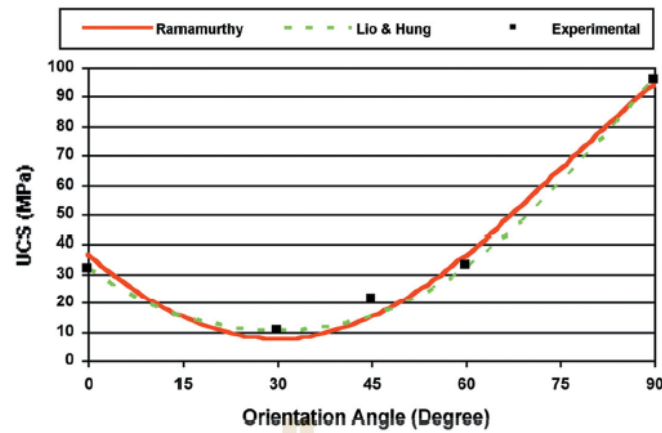


Figure 2.2 Strength results of Goshashi et al. (2006).

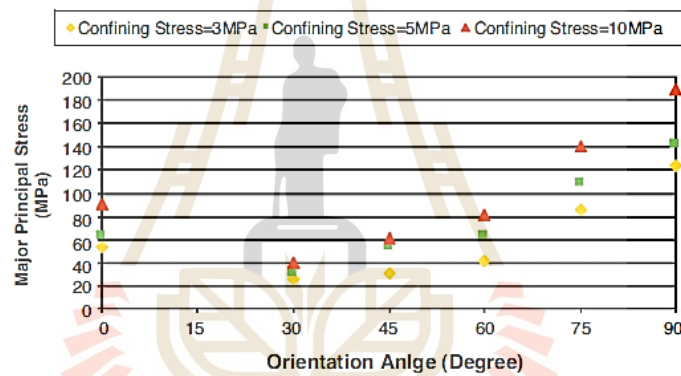


Figure 2.3 Strengths under different angles (Goshashi et al., 2006).

Figures 2.4 show the results between the predicted strengths and the test results under different confining pressures. Hoek and Brown and McLamore criteria can well predict the strength data.

The modified Hoek-Brown criterion is proposed by (Saroglou and Tsiambaos, 2008) and incorporating parameter (k_{β}) to consider the effect of strength anisotropy. The compression tests are performed on gneiss, schist and marble specimens in which the planes of anisotropy were from to 0° to 90° .

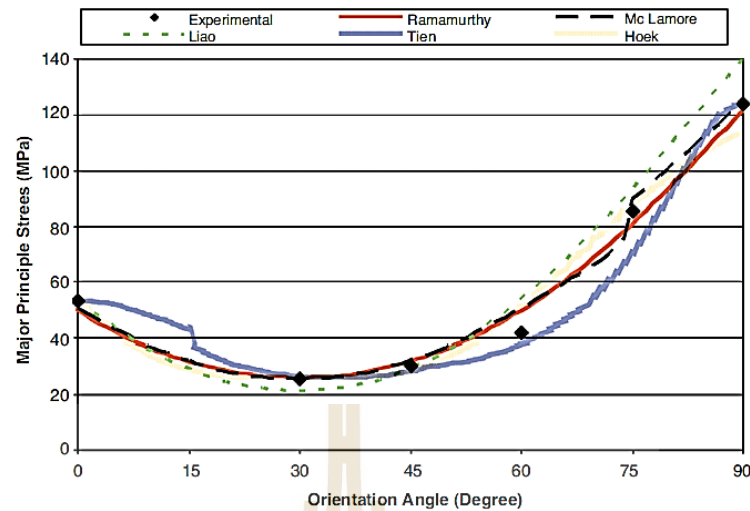


Figure 2.4 Comparison of Goshashi et al. (2006).

Cho et al. (2012) study the anisotropy behavior of Asan gneiss, Boryeong shale and Yeoncheon schist in Korea. The anisotropy ratios (maximum to minimum strengths) are 2.6, 2.6 and 18.6 for the gneiss, shale and schist. The anisotropy ratios of tensile strengths are 3.2, 2.2 and 7.1 for gneiss, shale and schist.

Miller et al. (2013) study the anisotropic effect on compressive strength of calcareous mudstone. The anisotropy decreases with increasing confining stress (Figure 2.5). Strength anisotropy is nearly identical to the anisotropy in the unloading modulus, with the material becoming isotropic under confining pressures.

2.3 Effect of Transverse Isotropy on Elastic Properties of Rocks

Hakala et al. (2007) study the anisotropy of Olkiluoto mica gneiss. Compared the elastic parameter from Amadei's solution with previous test results, the apparent Young's modulus and Poisson's ratio are similar.

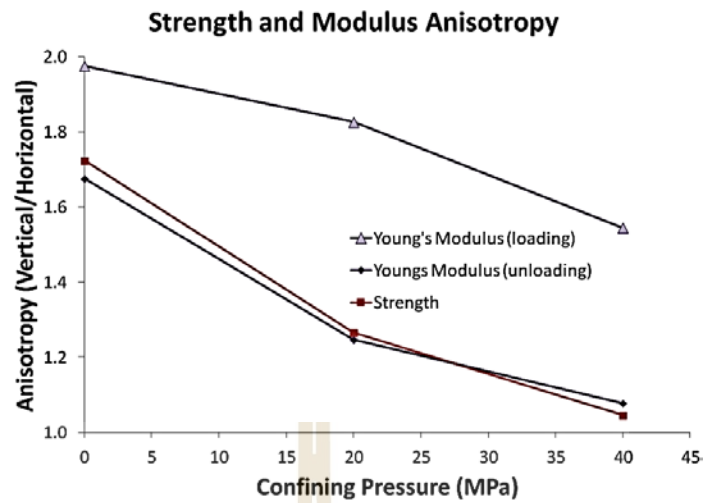


Figure 2.5 Results of Miller et al. (2013).

Miller et al. (2013) study the effect of anisotropy on static and dynamic elastic properties of a block of calcareous mudstone. The result indicate that the effect of anisotropy decreases under high confining pressures.

The results of Hu et al. (2017) indicate that rock mechanical behavior are affected by stress and rock anisotropy. The Young's modulus of sandstone at angle $\theta = 0^\circ$ was greater than that of $\theta = 90^\circ$ (Figure 2.6). The bedding plane at $\theta = 90^\circ$ closed under the application of axial stress and resulted in a high axial strain. A $\theta = 0^\circ$, the axial loading closes the matrix, and hence the axial strain becomes smaller. At $\theta = 30^\circ$, a sliding failure along bedding planes is observed. This axial strain larger than the other two axes.

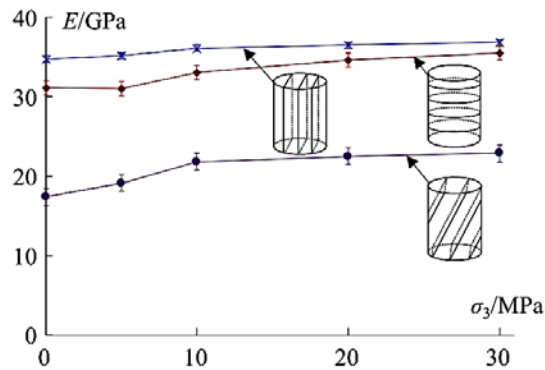


Figure 2.6 Results of Hu et al. (2017).

2.4 Analysis of Transversely Isotropic Effect on Elastic Property of Materials

Amadei (1996) propose solutions for transversely isotropic materials based on theory of elasticity. He assumes uniform stresses and strains in the test specimen. The strains ε_x , ε_y , ε_z and γ_{xy} can be related to the stress, σ , as follows :

$$\varepsilon_x = a_{12}\sigma; \quad \varepsilon_y = a_{22}\sigma; \quad \varepsilon_z = a_{23}\sigma; \quad \gamma_{xy} = a_{26}\sigma \quad (2.3)$$

with

$$a_{12} = -\frac{\nu'}{E} \sin^4 \theta - \frac{\nu'}{E} \cos^4 \theta + \frac{\sin^2 2\theta}{4} \left(\frac{1}{E} + \frac{1}{E'} - \frac{1}{G'} \right)$$

$$a_{22} = \frac{\cos^4 \theta}{E'} + \frac{\sin^4 \theta}{E} + \frac{\sin^2 2\theta}{4} \left(\frac{1}{G'} - \frac{2\nu'}{E'} \right)$$

$$a_{23} = -\frac{\nu'}{E} \cos^2 \theta - \frac{\nu}{E} \sin^2 \theta$$

$$a_{26} = \sin 2\theta \left[\cos^2 \theta \left(\frac{1}{E'} + \frac{\nu'}{E'} \right) - \sin^2 \theta \left(\frac{1}{E} + \frac{\nu'}{E'} \right) \right] - \frac{\sin 2\theta \cos 2\theta}{2G'} \quad (2.4)$$

Equations (2.3) and (2.4) can be used to calculate the apparent Young's modulus, E_y , and apparent Poisson's ratios ν_{yx} and ν_{yz} .

$$E_y = \frac{1}{a_{22}}; \quad \nu_{yx} = -\frac{a_{12}}{a_{22}}; \quad \nu_{yz} = -\frac{a_{23}}{a_{22}}. \quad (2.5)$$

Figure 2.7 gives an example of E_y , ν_{yx} and ν_{yz} under different anisotropic plane angle (θ).

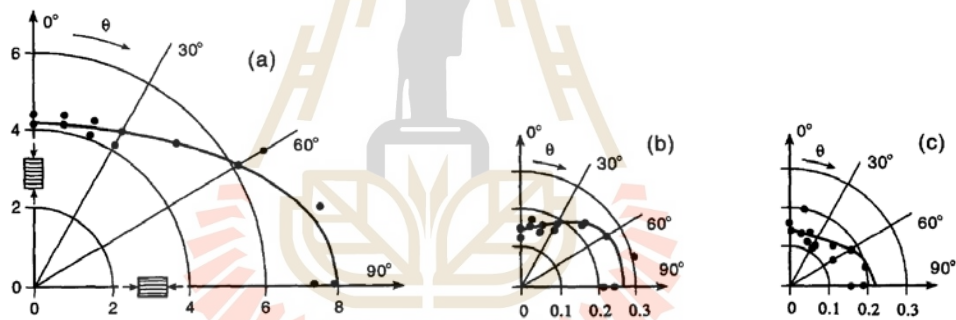


Figure 2.7 Examples of Amadei calculations.

The predictions (solid lines) agree with the test data. Figure 2.8 give the apparent Young's modulus under different angles θ . The simple model based on equations (2.3), (2.4) and (2.5) suggests that the elastic parameters of an anisotropic rock can vary widely if different specimens are cut in different orientations with respect to the anisotropy planes.

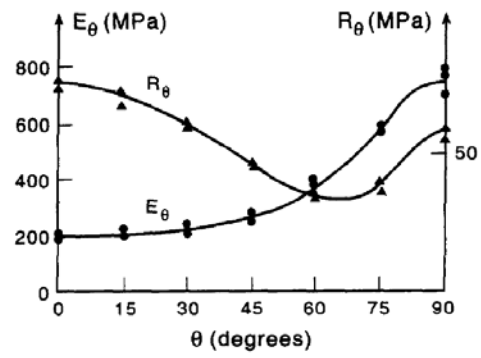


Figure 2.8 Young's modulus predicted by Amadei (1996).



CHAPTER III

SAMPLE PREPARATION

3.1 Introduction

This chapter describe sample preparation for the compression testing. The specimen dimensions are given. Mineral compositions of some specimens are determined by x-ray diffraction analysis.

3.2 Sample preparation

Salt blocks ($0.5 \times 0.5 \times 1.0 \text{ m}^3$) are collected from an underground mine opening of Thai Kali Co., Ltd. They belong to the Lower Salt member of the Maha Sarakham formation (Figure 3.1).

The specimens are virtually pure halite with slight amount of clay mineral and anhydrite inclusions (less than 1%). The average density is $2.16 \pm 0.09 \text{ g/cc}$. The salt blocks are cut using organic oil as lubricant to obtain rectangular specimens with nominal dimensions of $54 \times 54 \times 108 \text{ mm}^3$. Twenty-six specimens have been prepared. They contain different bedding plane orientations. The angles between the major axis and the normal to bedding planes (β) vary from 0, 25, 45, 60 to 90 degrees. Figure 3.2 shows pictures of some specimen. For all specimens, the bedding plane strike is parallel to one of the specimen sides. Sample preparation carried out in the laboratory at Suranaree University of Technology. Table 3.1 lists the specimen dimensions and orientations of bedding plane. The angle β measured between the normal to bedding plane and the major axis of the specimen.

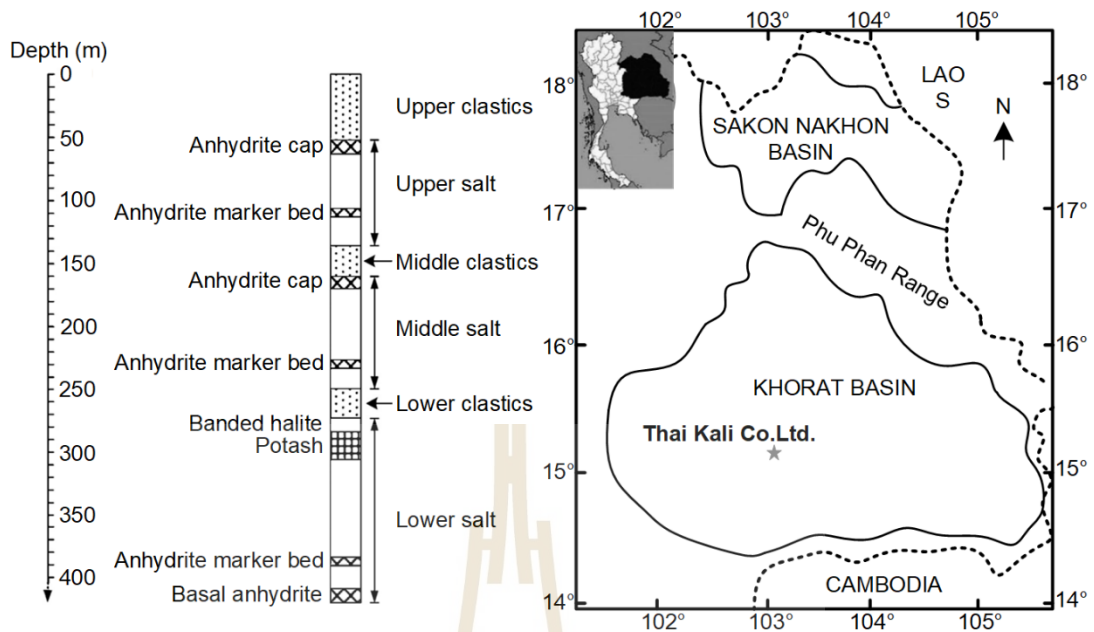


Figure. 3.1 Location of Thai Kali Co., Ltd. in Khorat salt basin and typical geologic sequence of Maha Sarakham formation at mine site.

The specimens are virtually pure halite with slight amount of clay mineral and anhydrite inclusions (less than 1%). The average density is 2.16 ± 0.09 g/cc. The salt blocks are cut using organic oil as lubricant to obtain rectangular specimens with nominal dimensions of $54 \times 54 \times 108$ mm³. Twenty-six specimens have been prepared. They contain different bedding plane orientations. The angles between the major axis and the normal to bedding planes (β) vary from 0, 25, 45, 60 to 90 degrees. Figure 3.2 shows pictures of some specimen. For all specimens, the bedding plane strike is parallel to one of the specimen sides. Sample preparation carried out in the laboratory at Suranaree University of Technology. Table 3.1 lists the specimen dimensions and orientations of bedding plane. The angle β measured between the normal to bedding plane and the major axis of the specimen.

Table 3.1 Salt specimens prepared for uniaxial and triaxial compression tests.

Specimen No.	Width (mm)	Length (mm)	Height (mm)	β (degrees)
LS-UCS-01	51.90	49.85	106.30	0
LS-UCS-02	54.62	54.52	108.10	25
LS-UCS-03	58.34	59.32	106.26	45
LS-UCS-04	53.98	54.30	109.36	60
LS-UCS-05	54.20	53.80	105.60	90
LS -TRI-01	52.57	55.19	108.56	0
LS -TRI-02	53.00	53.15	105.19	0
LS -TRI-03	54.00	53.35	109.00	0
LS -TRI-04	53.85	53.75	109.75	0
LS -TRI-05	58.27	57.75	107.02	0
LS -TRI-06	54.29	54.45	104.33	0
LS -TRI-07	55.40	55.45	109.10	25
LS -TRI-08	53.90	54.30	106.13	25
LS -TRI-09	52.46	54.78	105.35	25
LS -TRI-10	53.85	54.75	101.65	45
LS -TRI-11	53.38	54.03	106.58	45
LS -TRI-12	52.95	53.10	107.46	45
LS -TRI-13	54.51	55.06	108.50	60
LS -TRI-14	54.72	53.49	107.90	60
LS -TRI-15	55.75	55.04	108.23	60
LS -TRI-16	54.80	55.00	107.20	90
LS -TRI-17	51.70	52.80	108.05	90
LS -TRI-18	53.20	54.40	107.80	90
LS -TRI-19	53.6	53.95	109.45	90
LS -TRI-20	55.60	56.19	108.30	90
LS -TRI-21	56.33	52.77	108.49	90

3.3 X-ray diffraction analysis

The X-ray diffractometer (Bruker, D2 Phaser) has been used to determine mineral compositions of two salt specimens. Table 3.2 given the results.

Table 3.2 Results of X-ray diffraction analysis.

Sample No.	Halite (%)	Anhydrite (%)	Sylvite (%)	Gypsum (%)	Dickite (%)	Montmorillonite (%)	Illite (%)	Tachyhydrite (%)
1	95.48	0.31	0.36	1.69	0.31	0.64	0.79	0.42
2	95.52	0.24	0.26	1.96	0.01	0.97	0.55	0.49

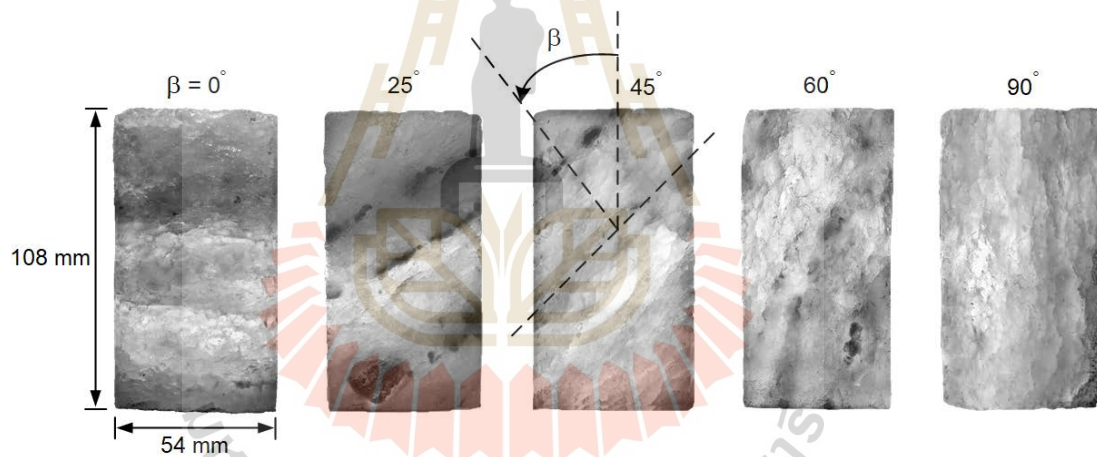


Figure. 3.2 Examples of specimens prepared for uniaxial compression and triaxial testing

CHAPTER IV

LABORATORY TESTING

4.1 Introduction

The objective of the laboratory testing is to physically reveal the effect of transverse isotropy on the strength and deformation properties of Maha Sarakham salt. Described in this chapter are the method and results of the laboratory testing. The tests are divided into two groups; uniaxial compression tests and triaxial compression tests. The results are combined to determine the effects of transverse isotropy on the compressive strength and elastic properties of the salt. The results obtained here are also compared with those supported elsewhere.

4.2 Test Methods

The uniaxial and triaxial compression tests are performed to determine the ultimate strength and the deformability under unconfined and confined conditions for various orientations of bedding planes in the salt specimens. A polyaxial load frame (Figure 4.1) is used to apply constant confining stresses to salt specimens while the axial stress is increased at the rate of 0.1 MPa/s until failure occurs. Exhaustive reviews of the polyaxial load frame have recently been given in Fuenkajorn et al. (2012). Except for the specimen geometry, the test procedure and calculation follow the ASTM D7012-14 (2014) standard practice. The testing system is calibrated before testing. In this study, the lateral stresses (σ_2 and σ_3) are equal ranging from 0, 5, 8 to 15 MPa, and the various orientations of bedding planes (β) varying from 0, 25, 45, 60 to 90 degrees,

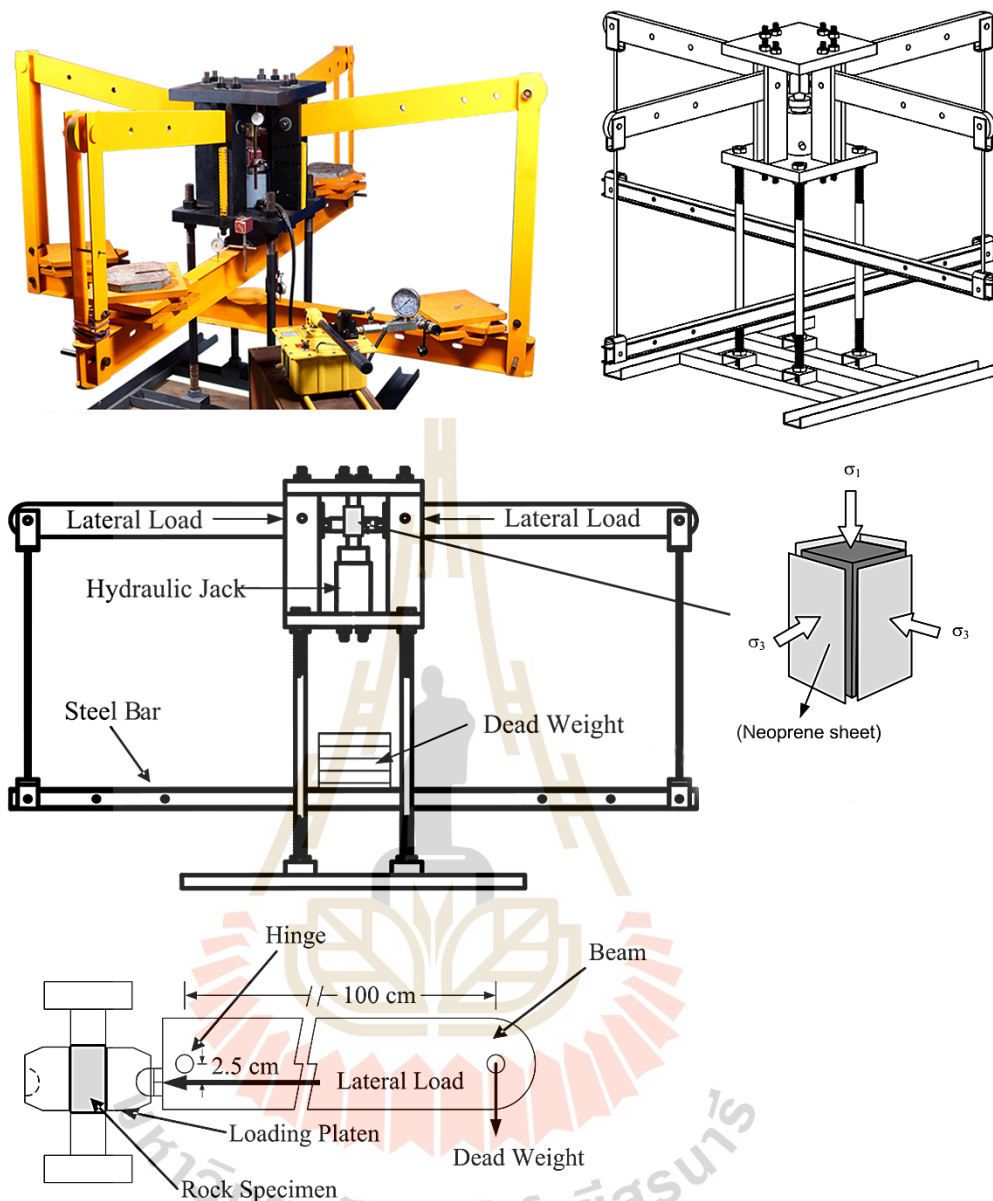


Figure 4.1 Polyaxial load frame employed in uniaxial and triaxial testing (Fuenkajorn et al., 2012).

where β is the angle between the specimen main axis and the normal to bedding planes. Neoprene sheets are used to reduce the friction at the interfaces between loading platens and rock surfaces. Figure 4.2 shows the applied principal stress directions with respect to the bedding planes. Note that all specimens have been prepared such that the bedding

plane strike is parallel to one of the specimen side. After installing the rectangular specimen into load frame, dead weights are placed on the steel bar to obtain a predefined lateral stresses (σ_3) on the specimen. The test is started by increasing the vertical stress at the rate of 0.1 MPa/s using a hydraulic pump. The digital displacement gages are used to measure axial and lateral deformations until failure occurs. The load at failure and modes of failure are identified. They are used to calculate the strength and deformation moduli of the salt.

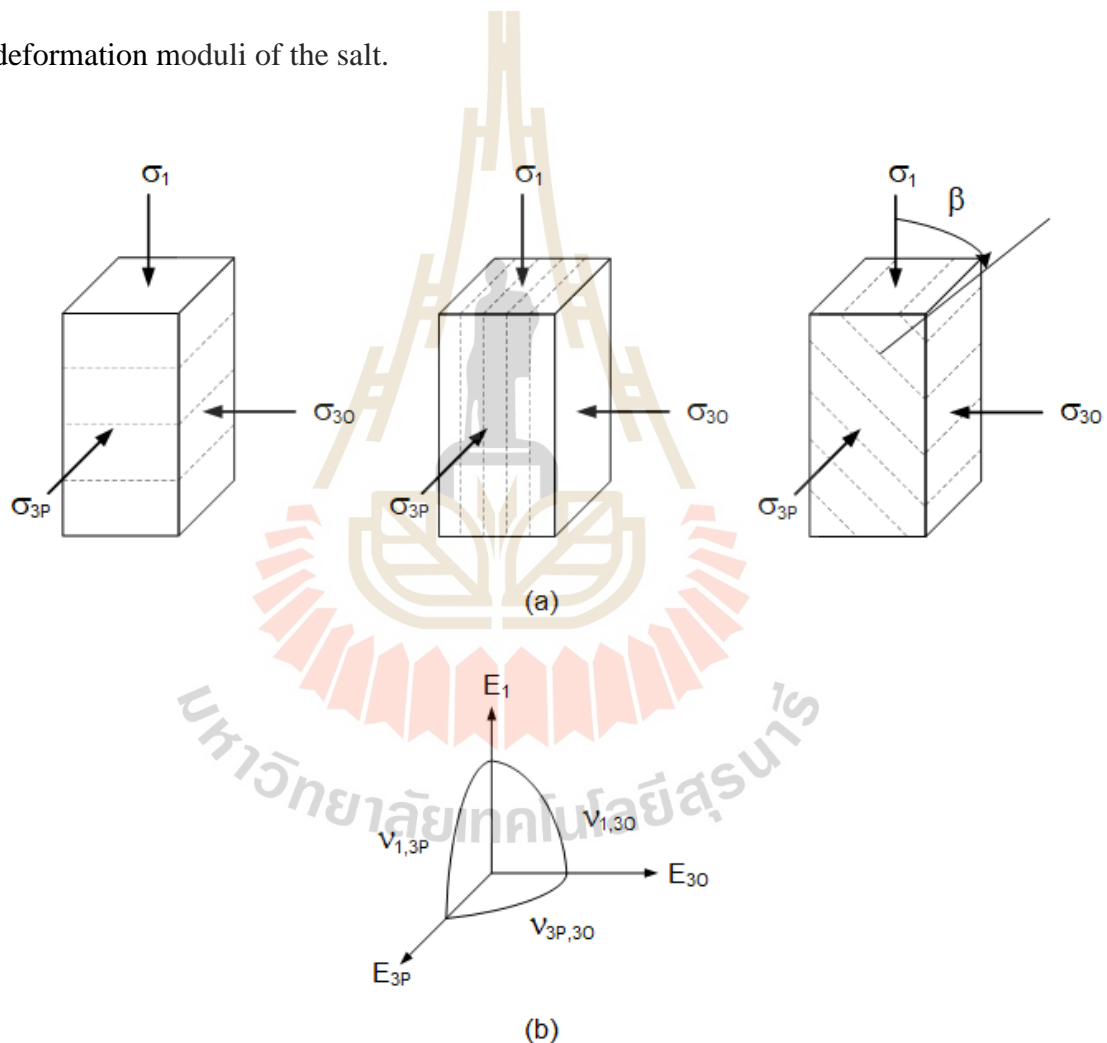


Figure 4.2 Loading directions with respect to bedding planes (a). Elastic parameters for transversely isotropic conditions (b).

4.3 Test results

All post-test specimens of uniaxial compression testing show plane failures along the salt bedding (Figure 4.3). Under uniaxial stress, the transverse elastic moduli along major principal (axial) direction (E_1) and along the two minor principal axes that are normal (E_{3O}) and parallel (E_{3P}) to bedding planes are calculated from the set of equations modified from those of Jaeger et al. (2007) as follows:

$$\varepsilon_1 = \sigma_1 / E_1 - (v_{1,3P} \sigma_{3P}) / E_{3P} - (v_{1,3O} \sigma_{3O}) / E_{3O} \quad (4.1)$$

$$\varepsilon_{3P} = - (v_{1,3P} \sigma_1) / E_1 + \sigma_{3P} / E_{3P} - (v_{3P,3O} \sigma_{3O}) / E_{3O} \quad (4.2)$$

$$\varepsilon_{3O} = - (v_{1,3O} \sigma_1) / E_1 - (v_{3P,3O} \sigma_{3P}) / E_{3P} + \sigma_{3O} / E_{3O} \quad (4.3)$$

where σ_1 is the major principal stress, σ_{3O} and σ_{3P} are the minor principal stresses that are normal and parallel to the strike of bedding planes, ε_1 is the major principal strain, ε_{3O} and ε_{3P} are the minor principal strains measured normal and parallel to the strike of bedding planes, $v_{1,3P}$ and $v_{1,3O}$ are Poisson's ratio's between major principal axis and the directions that are parallel and normal to the strike of beds, and $v_{3P,3O}$ is Poisson's ratio between directions that are parallel and normal to strike of beds. The transverse elastic moduli and Poisson's ratios under triaxial stresses condition can be, however, calculated only for the conditions where $\beta = 0$ and 90 degrees because beyond these conditions, the unknowns are more than the number of equations, and hence they become indeterminate. The failure stresses and calculated results are summarized in Table 4.1.

Figures 4.4 through 4.8 shows the stress–strain curves monitored from the test specimens under various confining pressures and bedding orientations. The effect of

transverse isotropic on lateral strain can be clearly observed by increasing β . The variation of strengths with loading orientations shows U-shaped anisotropy curve where the strength is largest when loading is normal to the anisotropic plane and the lowest strength occurs when $\beta = 60$ degrees (Figure 4.9). This observation is also found from the rock specimens with one set of discontinuity by Al-Harhi (1998), especially under lower confining pressures.

Table 4.1 Compression test results.

Orientation	$\sigma_{3P} = \sigma_{3O}$ (MPa)	$\sigma_{1,f}$ (MPa)	E_1 (GPa)	E_{3P} (GPa)	E_{3O} (GPa)	$\nu_{1,3P}$	$\nu_{1,3O}$	$\nu_{3P,3O}$
$\beta = 0^\circ$	0	25.1	1.35	2.40	2.40	0.35	0.35	0.32
	2	43.1	1.46	2.42	2.42	0.35	0.35	0.32
	3	51.2	1.60	2.42	2.42	0.34	0.34	0.31
	5	60.3	1.72	2.43	2.43	0.34	0.34	0.32
	8	70.3	2.01	2.45	2.45	0.33	0.33	0.31
	12	80.5	2.16	2.45	2.45	0.33	0.33	0.32
	15	87.2	2.37	2.46	2.46	0.31	0.32	0.32
$\beta = 25^\circ$	0	19.3	1.46	1.51	1.46	0.33	0.35	0.32
	5	56.6	-	-	-	-	-	-
	8	68.0	-	-	-	-	-	-
	15	86.3	-	-	-	-	-	-
$\beta = 45^\circ$	0	13.6	1.61	1.71	1.61	0.33	0.35	0.34
	5	50.2	-	-	-	-	-	-
	8	62.9	-	-	-	-	-	-
	15	82.9	-	-	-	-	-	-
$\beta = 60^\circ$	0	11.4	1.92	2.04	1.92	0.32	0.36	0.33
	5	46.9	-	-	-	-	-	-
	8	60.7	-	-	-	-	-	-
	15	81.3	-	-	-	-	-	-
$\beta = 90^\circ$	0	16.3	2.40	2.40	1.35	0.31	0.36	0.36
	2	32.1	2.42	2.42	1.45	0.31	0.36	0.36
	3	43.5	2.42	2.42	1.60	0.32	0.35	0.35
	5	53.9	2.43	2.43	1.72	0.31	0.34	0.34
	8	65.4	2.45	2.45	2.02	0.31	0.33	0.33
	12	77.8	2.45	2.45	2.15	0.32	0.33	0.33
	15	85.4	2.46	2.46	2.37	0.32	0.32	0.32

Note: Since specimens are not isotropic, their elastic parameter for $0^\circ < \beta < 90^\circ$ under $\sigma_3 > 0$ can not be determined from measurements.

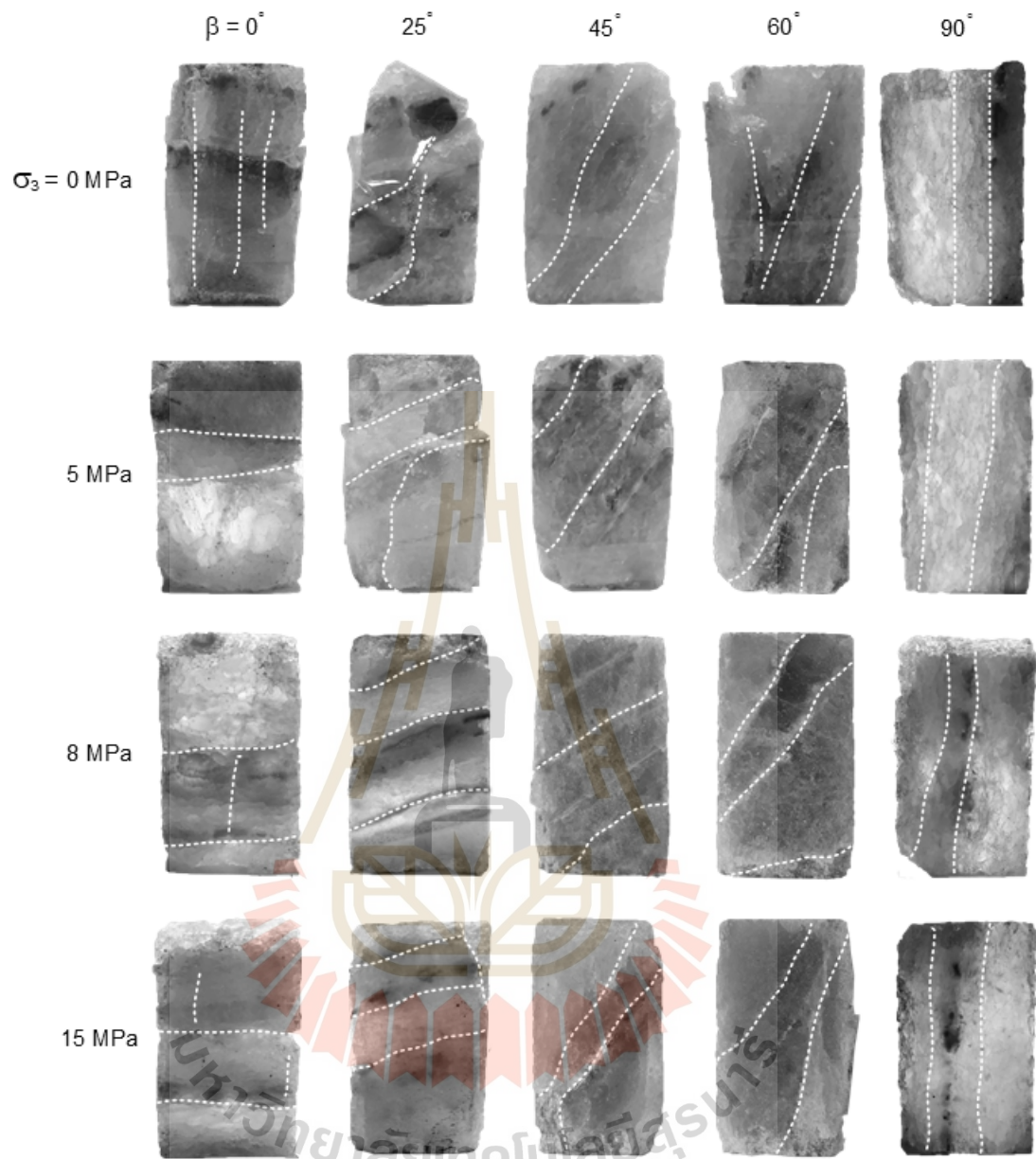


Figure 4.3 Some post-test specimens of uniaxial and triaxial compression test. White lines indicate induced fractures.

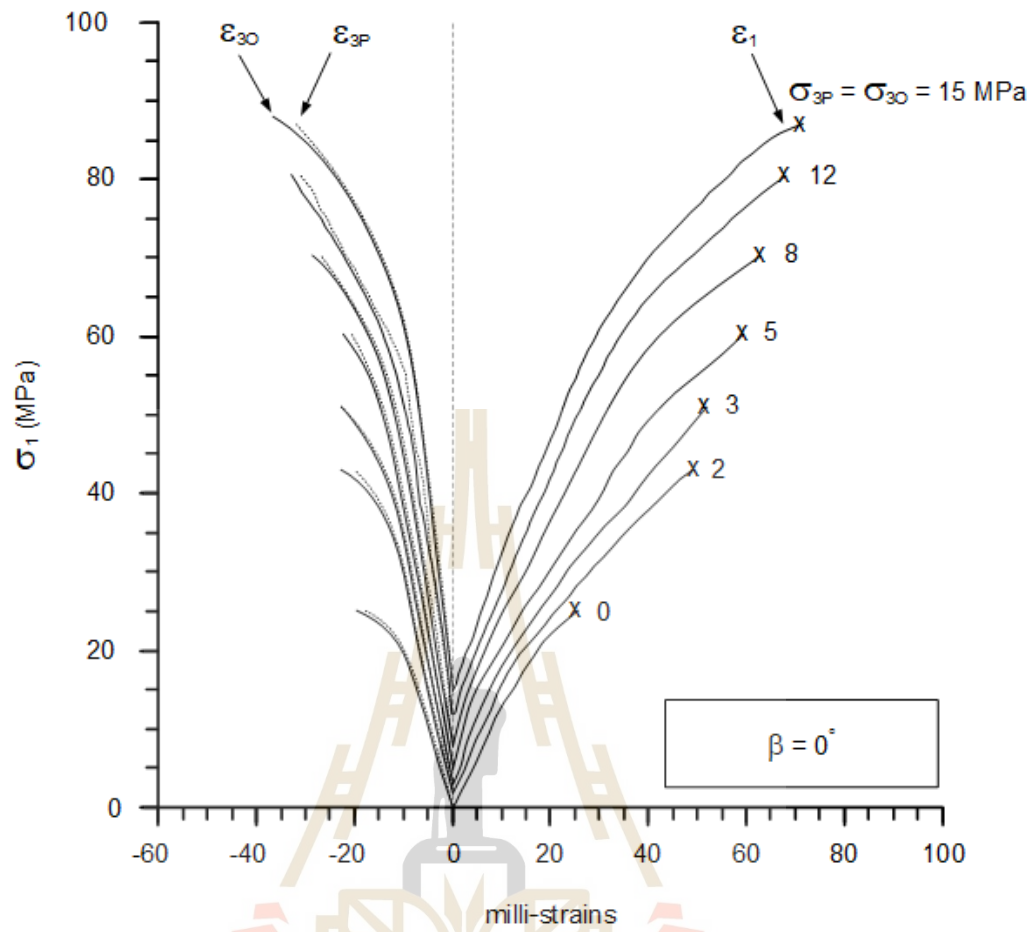


Figure 4.4 Stress-strain curves from compression tests on salt specimens with $\beta = 0^\circ$ shows notations used in stress-strain diagrams.

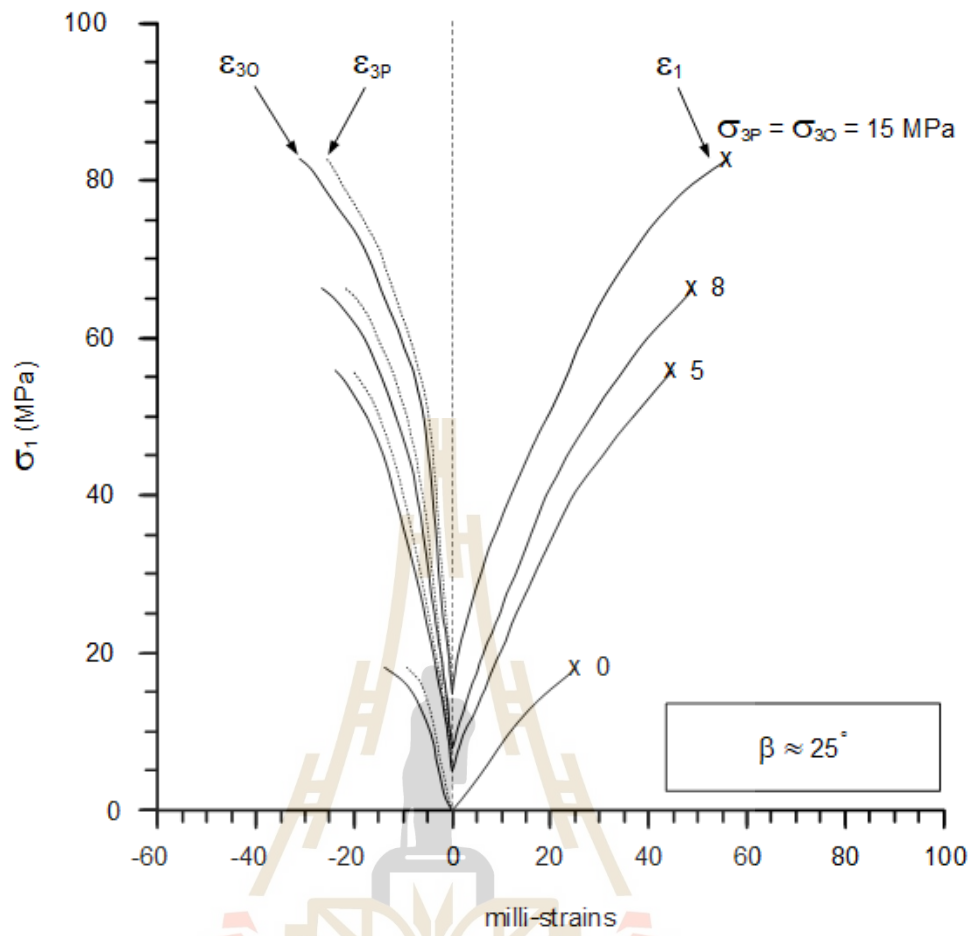


Figure 4.5 Stress-strain curves from compression tests on salt specimens with $\beta \approx 25^\circ$ shows notations used in stress-strain diagrams.

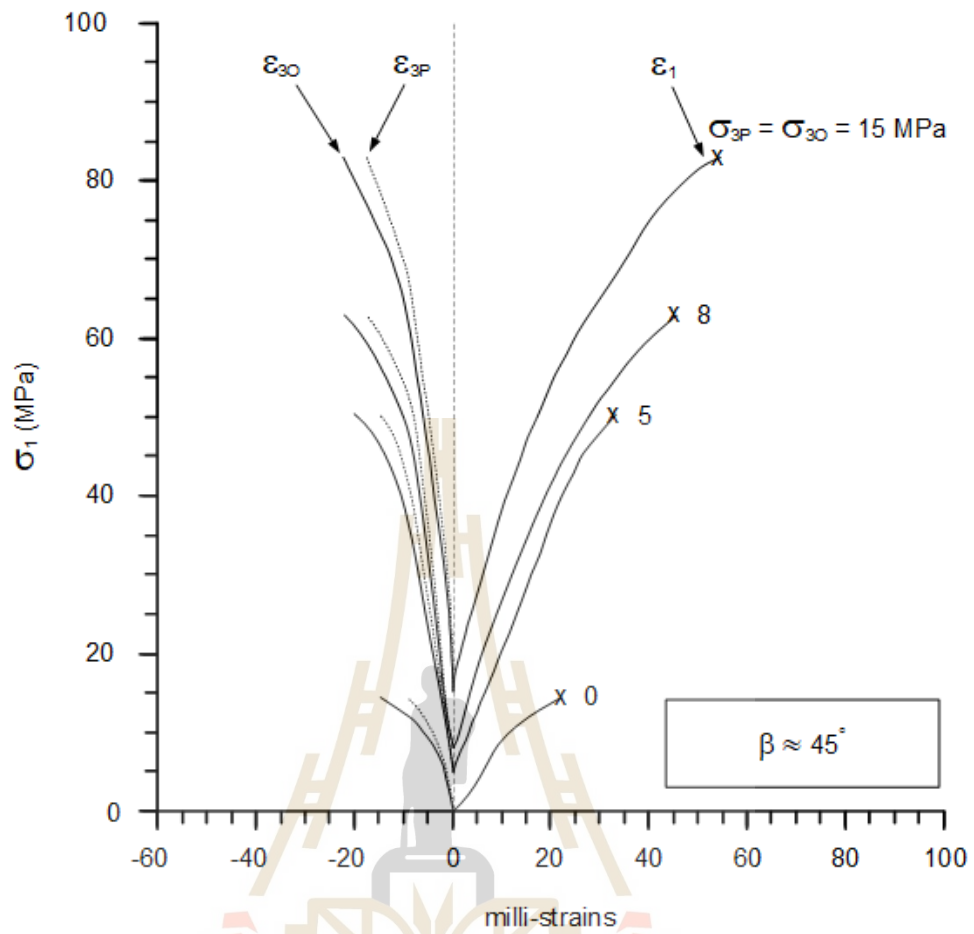


Figure 4.6 Stress-strain curves from compression tests on salt specimens with $\beta \approx 45^\circ$ shows notations used in stress-strain diagrams.

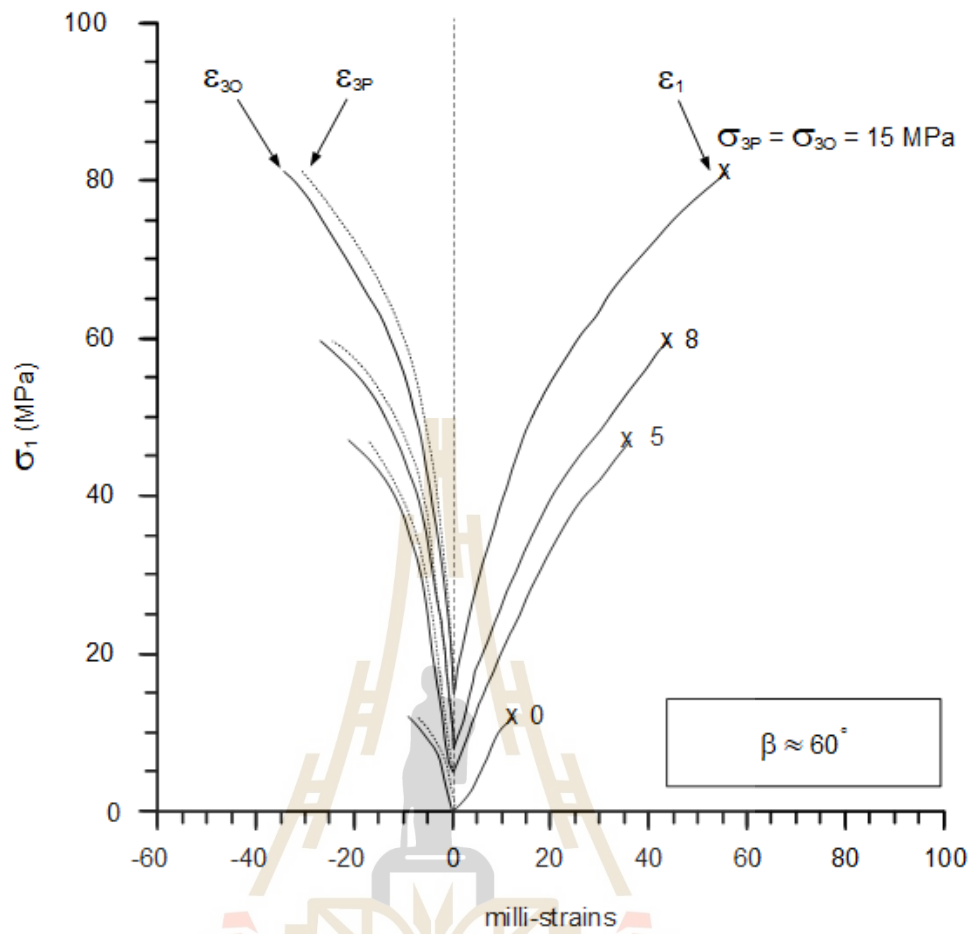


Figure 4.7 Stress-strain curves from compression tests on salt specimens with $\beta \approx 60^\circ$ shows notations used in stress-strain diagrams.

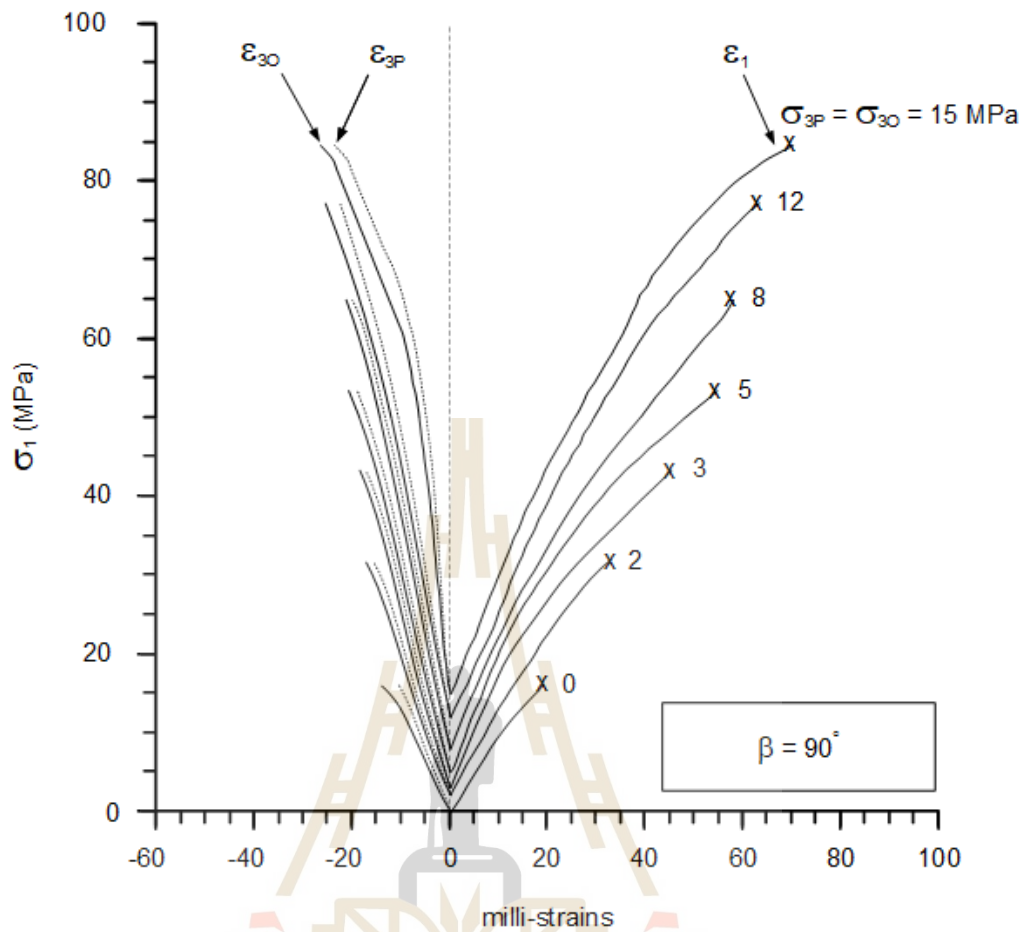


Figure 4.8 Stress-strain curves from compression tests on salt specimens with $\beta = 90^\circ$ shows notations used in stress-strain diagrams.

Figure 4.10 shows the elastic moduli as a function of β for different confining pressures (σ_3). The results indicate that the elastic modulus increases with increasing β , especially under uniaxial condition. Under high confining pressures, the effect of transverse isotropic on bedded salt specimens tends to decrease. This is because the specimens can be self-healed, and hence they can be restored to the homogeneous rocks.

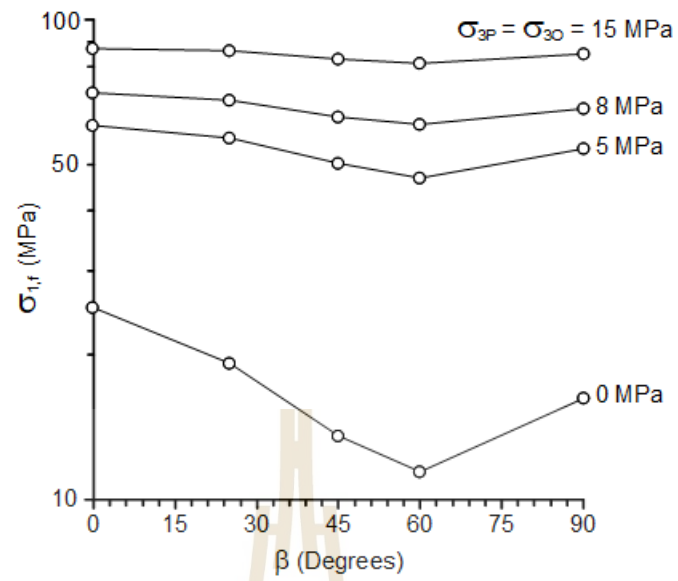


Figure 4.9 Compressive strengths as a function of β for different confining pressures

(σ_3).

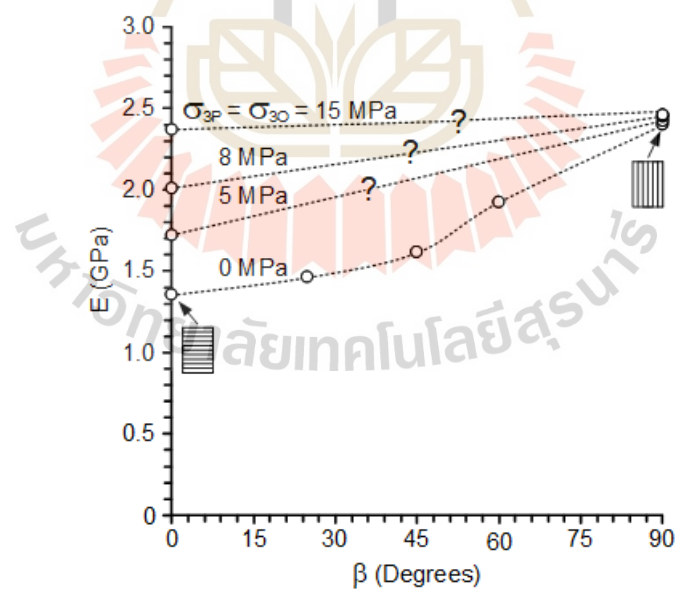


Figure 4.10 Elastic moduli as a function of β for different confining pressures (σ_3).

CHAPTER V

STRENGTH CRITERIA

5.1 Introduction

This chapter presents the strength results obtained from uniaxial and triaxial compression testing. Hoek-Brown, Coulomb and strain energy criteria are used to describe the strength data obtained from various bedding orientations. The criteria incorporate the effect of transverse isotropy caused by the bedding planes, which can be applied to determine the salt strengths under in-situ conditions.

5.2 Hoek and Brown criterion

Hoek–Brown criterion (Hoek and Brown, 1980) describes the relationship between the major (σ_1) and minor (σ_3) principal stresses at failure of the triaxial test results:

$$\sigma_1 = \sigma_3 + (m\sigma_c'\sigma_3 + s\sigma_c'^2)^{1/2} \quad (5.1)$$

where σ_c' is the uniaxial compressive strength, and m and s are material constants. Constant m is depending on the properties of rock and $s = 1$ for intact rocks. The criterion has long been used to describe the strength of intact rock and rock mass, particularly for those that have anisotropic properties. Regression analysis has been performed on the strength data based on the failure criterion given in equation (5.1). Figure 5.1 shows the failure envelopes for different loading orientations with respect to the bedding planes.

The results indicate that the strengths increase with increasing confining pressure. The maximum compressive strength is obtained for $\beta = 0^\circ$. For $\beta = 60^\circ$, the strength is lowest. The parameter m varies with the orientations β as shown in Table 5.1. Failure envelopes in Figure 5.1 suggest that the effect of transversely isotropy could gradually decrease when the rocks are subjected to higher confining pressures and could reach the isotropic and homogeneous conditions under $\sigma_{30} = \sigma_{3P}$ of about 30 MPa.

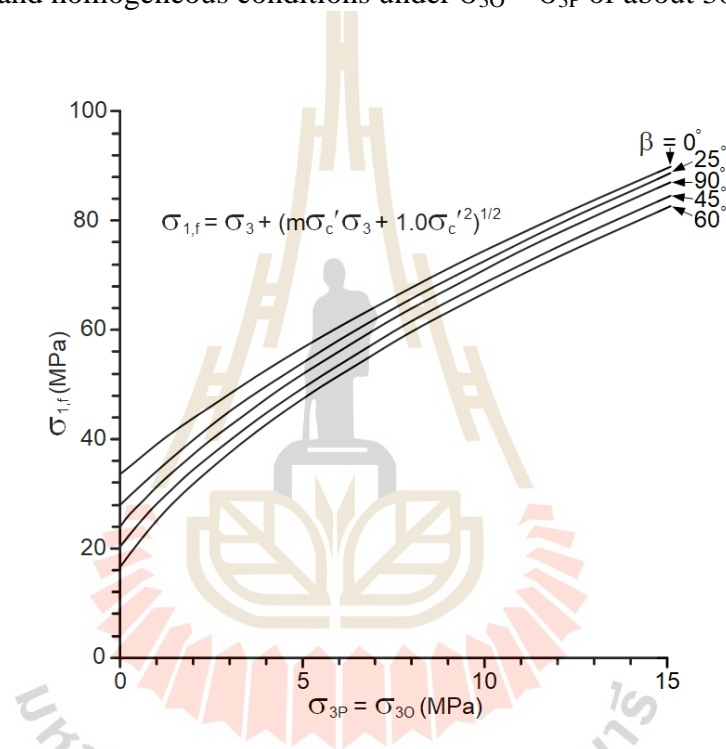


Figure 5.1 Hoek–Brown criterion of salt specimens with different bedding plane angles.

Table 5.1 Orientation angles and their constants calibrated from compression test data.

β (Degrees)	σ_c' (MPa)	m	R^2
0	33.4	8.89	0.935
25	27.9	11.04	0.956
45	20.4	14.38	0.982
60	16.4	17.30	0.990
90	24.1	12.68	0.973

The constant m and the calculated uniaxial compressive strength (σ_c) vary with angle β . Via regression analysis, their relationships can be expressed in the forms of polynomial equations, as follows:

$$m = (-7.00 \times 10^{-5}) \cdot \beta^3 + (7.20 \times 10^{-3}) \cdot \beta^2 + (-4.65 \times 10^{-2}) \cdot \beta + m_{(0)} \quad (5.2)$$

$$\sigma_c' = (8.00 \times 10^{-5}) \cdot \beta^3 + (-5.90 \times 10^{-3}) \cdot \beta^2 + (-1.92 \times 10^{-1}) \cdot \beta + \sigma_{c(0)} \quad (\text{MPa}) \quad (5.3)$$

where $m_{(0)}$ is a material constants at $\beta = 0^\circ$ and $\sigma_{c(0)}$ is the uniaxial compressive strength at $\beta = 0^\circ$. The polynomial equations fit well to the parameter m and σ_c' results, with R^2 greater than 0.9. Figure 5.2 plots the parameter m and calculated uniaxial compressive strength (σ_c') as a function of β varying from 0 to 90 degrees.

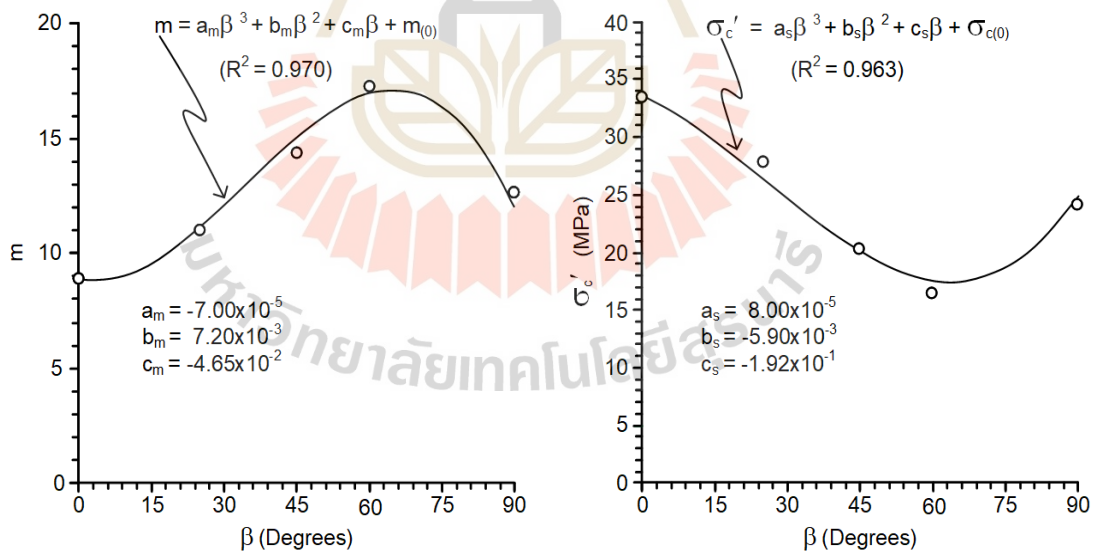


Figure 5.2 Hoek-Brown parameter m (a) and calculated uniaxial compressive strength σ_c (b) as a function of β .

Figure 5.3 shows the strengths (σ_c) obtained from uniaxial compression test as a function of calculated strength (σ_c') from Hoek and Brown criteria. The linear equations fit well to the σ_c and σ_c' results, with R^2 greater than 0.9.

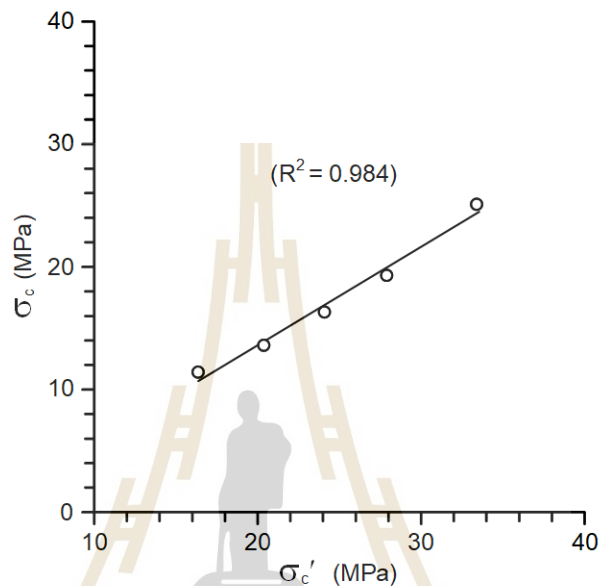


Figure 5.3 Uniaxial compressive strength (σ_c) as a function of calculated strength (σ_c').

5.3 Coulomb criterion

Based on the Coulomb strength criterion, the internal friction angle (ϕ) and cohesion (c) of rock salt specimens can be determined for each bedding plane orientation. The Coulomb strength criterion can be written as (Jaeger et al., 2007):

$$\sigma_1 = \sigma_c + \sigma_3 \tan 2\phi \quad (5.4)$$

$$c = \sigma_c / (2 \tan \phi) \quad (5.5)$$

$$\phi = 2 \alpha - (\pi/2) \quad (5.6)$$

The cohesion and friction angle of intact salt can be obtained from regression analyses of the uniaxial compressive strength and a set of major (σ_1) and minor (σ_3) principal stresses at failure obtained under different orientation angles. The regression results show good correlations ($R^2 > 0.9$) between the criterion and the test data. The parameter α is then used to calculate the friction angle and cohesion by using equations (5.5) and (5.6). The ϕ and c values for each angle are summarized in Table 5.2, and are plotted as a function of the confining stresses (σ_3) in Figure 5.4. The cohesions tend to decrease with increasing angle β . The internal friction angles, however, tend to increase with angle β in Figure 5.5. Another form of the Coulomb criterion, the shear strength (τ) can be represented by:

$$\tau = c + \sigma_n \tan \phi \quad (5.7)$$

where σ_n is normal stress, ϕ is friction angle and c is cohesion.

Table 5.2 Friction angles and cohesions for difference orientation angles from the test data.

β (Degrees)	ϕ (Degrees)	c (MPa)	R^2
0	30.73	10.01	0.927
25	38.61	6.57	0.919
45	39.51	4.93	0.935
60	39.78	4.26	0.944
90	38.84	6.08	0.941

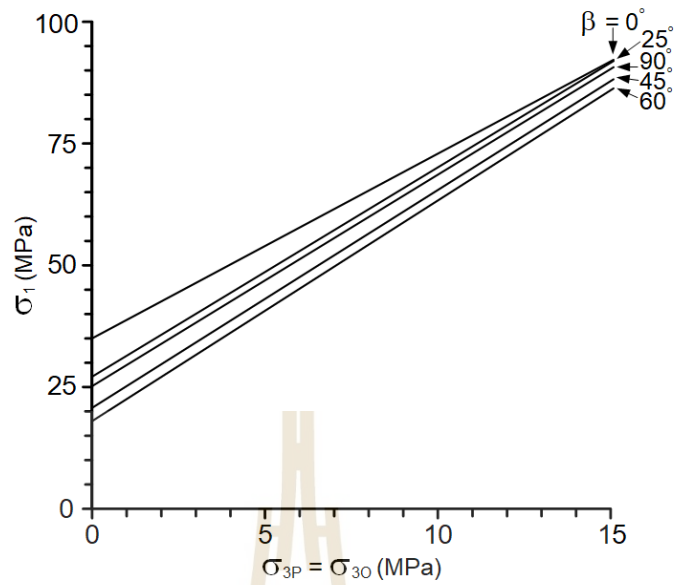


Figure 5.4 Maximum principal stress (σ_1) as a function of confining stress (σ_3) at failure for various orientation angles.

The cohesion (c) and friction angle (ϕ) of intact salt vary with angle β . Via regression analysis, polynomial equations can represent their relation as follows:

$$c = (8.00 \times 10^{-6}) \cdot \beta^3 + (5.00 \times 10^{-4}) \cdot \beta^2 + (-1.52 \times 10^{-1}) \cdot \beta + c_{(0)} \quad (\text{MPa}) \quad (5.8)$$

$$\phi = (4.00 \times 10^{-5}) \cdot \beta^3 + (-8.10 \times 10^{-3}) \cdot \beta^2 + (4.82 \times 10^{-1}) \cdot \beta + \phi_{(0)} \quad (\text{degrees}) \quad (5.9)$$

where $c_{(0)}$ is a cohesion at $\beta = 0^\circ$ and $\phi_{(0)}$ is the friction angle at $\beta = 0^\circ$. The polynomial equations fit well to the cohesion and friction angle, with R^2 greater than 0.9. Figure 5.5 plots the cohesion and friction angle as a function of β varying from 0 to 90 degrees.

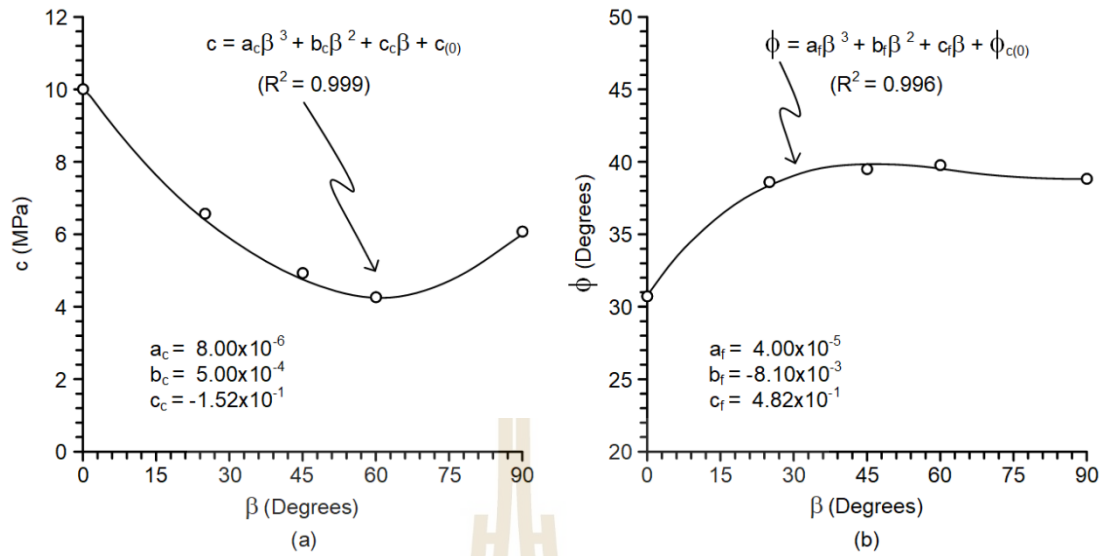


Figure 5.5 Cohesion, c (a) and internal friction angel, ϕ (b) as a function as of β .

5.4 Strength criterion based on strain energy density

The strain energy density principle is applied here to describe the rock salt strength and deformation under different orientation angles. The distortional strain energy (W_d) at failure can be calculated from the octahedral shear stresses and octahedral shear strain obtained from compression test data for each rock salt specimen, as follows (Jaeger et al., 2007):

$$W_d = (3/2)\tau_{oct}\gamma_{oct} \quad (5.10)$$

where γ_{oct} and τ_{oct} are octahedral shear strains and octahedral shear stresses at failure. The mean stress at failure (σ_m) can be calculated from axial stress (σ_1) and confining pressure (σ_3) for each salt specimen using the following relation (Jaeger et al., 2007):

$$\sigma_m = (\sigma_1 + 2\sigma_3) / 3 \quad (5.11)$$

The calculated W_d - σ_m relations at failure can be represented by a linear relation, as shown in Figure 5.6 which can be best represented by:

$$W_d = K\sigma_m \quad (5.12)$$

The parameters K is empirical parameters. The linear equations fit well to the W_d and σ_m results, with R^2 greater than 0.9. The parameter K varies with the orientations β as shown the results indicate that the parameter K decrease with increasing orientations. The maximum parameter K is obtained for $\beta = 0^\circ$. For $\beta = 60^\circ$, the parameter K is lowest. The W_d - σ_m relation above can be used as a strength criterion, where it implicitly considers the transversely isotropic strength of the salt. It's therefore more suitable to describe the salt pillar or salt wall stability in the mine, as compared to the conventional strength criteria that exclude transversely isotropic effect. Results for the octahedral shear strains (γ_{oct}), octahedral shear stresses (τ_{oct}), distortional strain energy density (W_d) and mean stress (σ_m) at failure are interpreted from these curves and listed in Tables 5.3.

5.5 Discussions of the test results

The results of strength criterion representations indicate that the strengths increase with increasing confining pressure. It also suggests the strength criteria may follow closely the Hoek–Brown criterion, as non-linear σ_1 and σ_3 curves are clearly observed. Therefore, the Mohr–Coulomb criterion may be used only as an approximation in the low confining pressure range. For a wider range of confining pressures, Hoek–Brown criterion should be applied to the test results. Figures 5.7

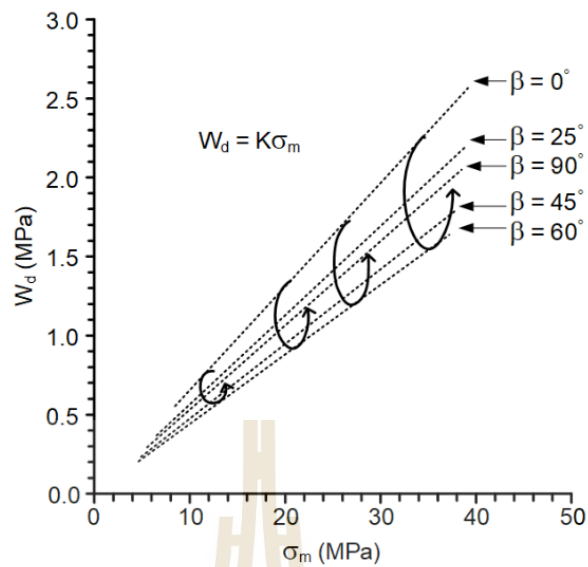


Figure 5.6 Distortional strain energy (W_d) at failure as a function mean stress (σ_m)

Table 5.3 Strain energy of each specimen.

β (Degrees)	σ_3 (MPa)	σ_m (MPa)	W_d (MPa)	K	R ²
0	0	8.37	0.37	0.066	0.987
	5	23.43	1.52		
	8	28.77	1.92		
	15	39.06	2.58		
25	0	6.44	0.24	0.056	0.992
	5	22.20	1.25		
	8	28.00	1.58		
	15	38.75	2.21		
45	0	4.82	0.14	0.053	0.988
	5	20.07	0.92		
	8	26.29	1.23		
	15	37.64	1.82		
60	0	4.55	0.10	0.047	0.993
	5	18.95	0.77		
	8	25.56	1.14		
	15	37.09	1.67		
90	0	5.43	0.16	0.044	0.987
	5	21.28	1.19		
	8	27.14	1.47		
	15	38.38	2.01		

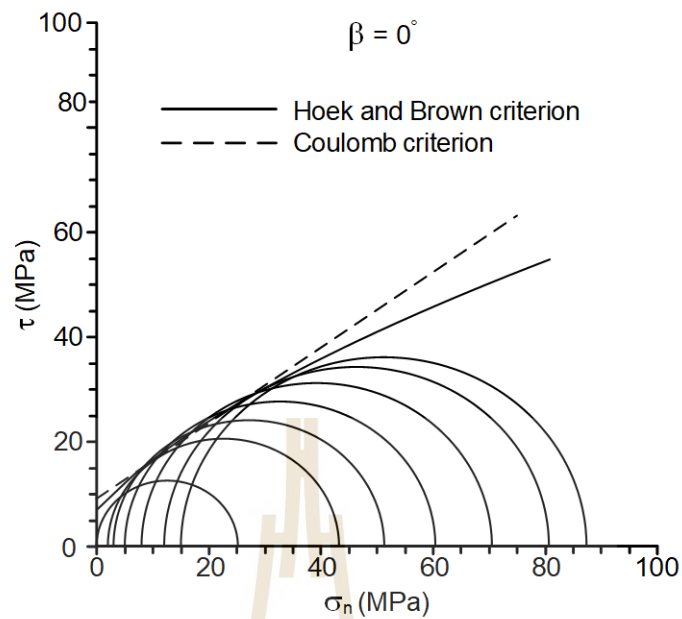


Figure 5.7 Mohr's circles from triaxial compressive strength tests on salt specimens with $\beta = 0^\circ$ in forms of Coulomb and Hoek–Brown criteria.

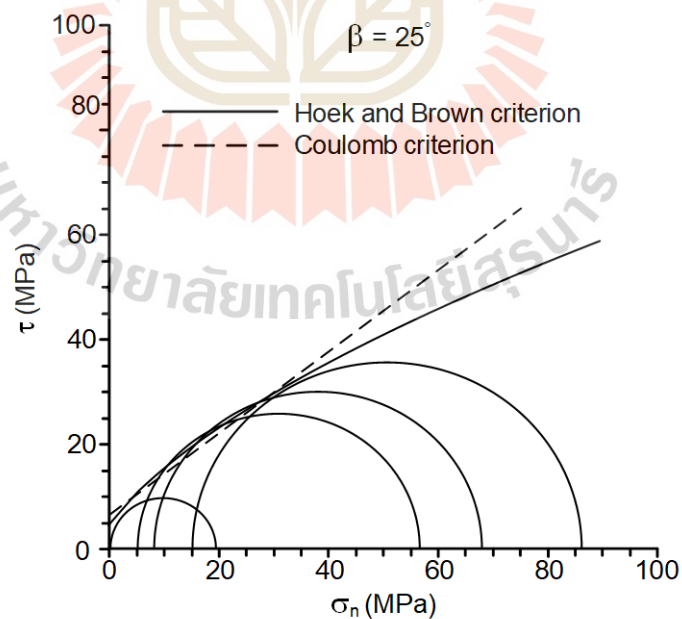


Figure 5.8 Mohr's circles from triaxial compressive strength tests on salt specimens with $\beta = 25^\circ$ in forms of Coulomb and Hoek–Brown criteria.

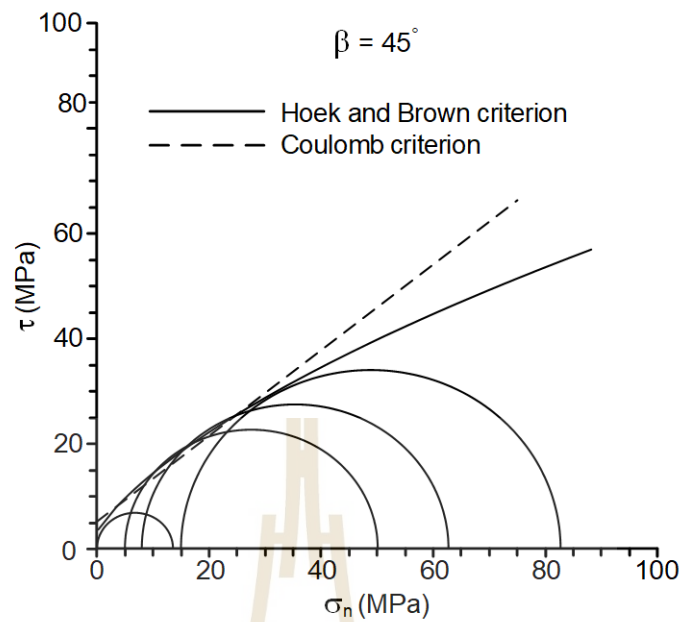


Figure 5.9 Mohr's circles from triaxial compressive strength tests on salt specimens with $\beta = 45^\circ$ in forms of Coulomb and Hoek–Brown criteria.

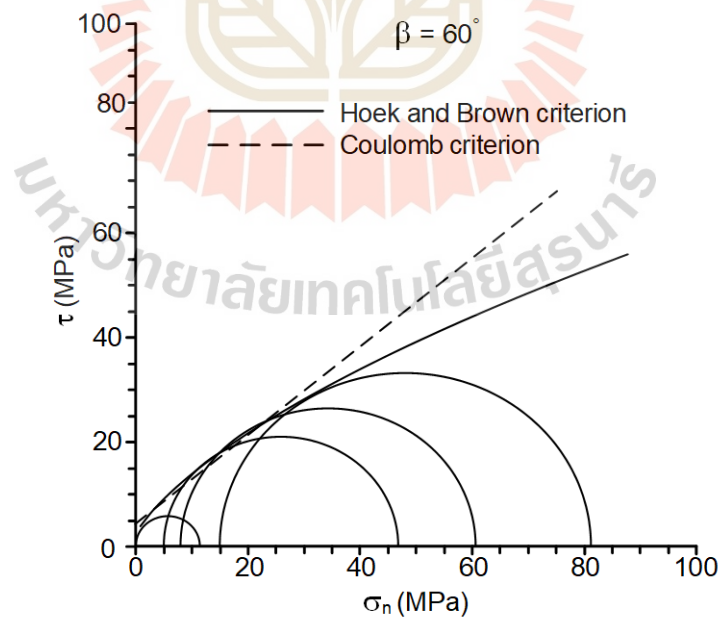


Figure 5.10 Mohr's circles from triaxial compressive strength tests on salt specimens with $\beta = 60^\circ$ in forms of Coulomb and Hoek–Brown criteria.

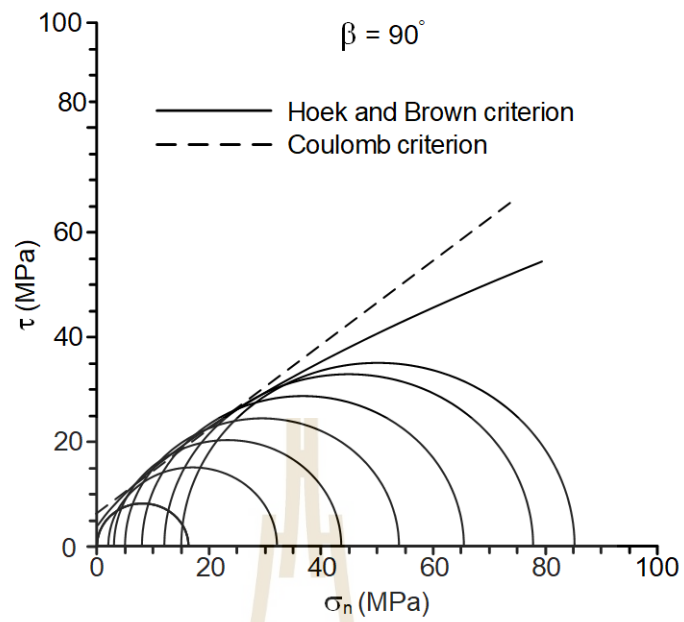
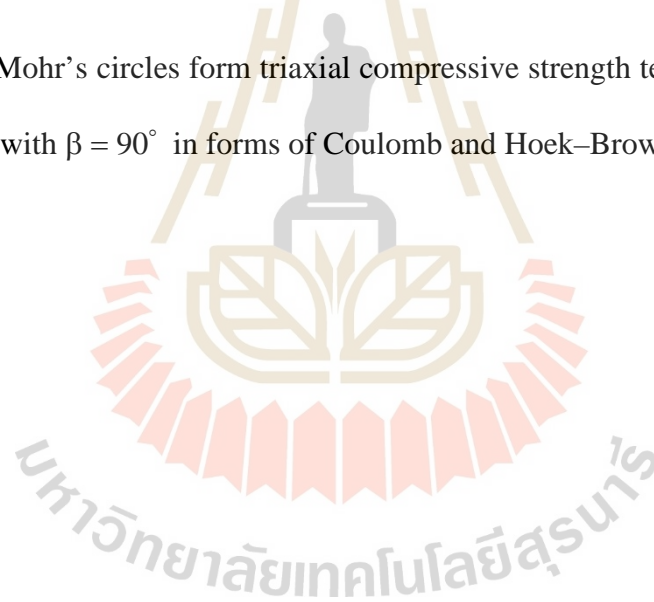


Figure 5.11 Mohr's circles from triaxial compressive strength tests on salt specimens with $\beta = 90^\circ$ in forms of Coulomb and Hoek–Brown criteria.



CHAPTER VI

TRANSVERSELY ISOTROPIC EFFECT ON SALT

ELASTICITY

6.1 Introduction

An attempt is made here to determine the elastic parameters (elastic modulus and Poisson's ratio) under varied directions with respect to the orientations of bedding planes. An approximate solutions proposed by Amadei (1996) have been applied. This chapter presents a determination of rock anisotropy, and the calculations of the approximate values of elastic modulus and Poisson's ratio.

6.2 Degrees of rock anisotropy

Several investigators (Gerrard, 1975; Batugin and Nirenburg, 1972; Amadei et al., 1987; Ramamurthy, 1993; Hakala et al., 2007) have determined the degrees of rock anisotropy using the ratio of E (maximum elastic moduli in the plane of transverse isotropy) to E' (minimum elastic moduli in direction normal to the plane of transverse isotropy). The high values of E/E' ratio indicate the stronger degree of anisotropy. Based on the test results reported in previous chapter, the E/E' ratios of Maha Sarakham salt have been calculated. The results are given in Table 6.1. The ratios are also plotted as a function of confining pressure in Figure 6.1. The anisotropic ratios reduce from 1.78 under unconfined condition ($\sigma_3 = 0$) to 1.04 under confining pressure of 15 MPa.

The diagram in the figure suggests that the salt tends to become more isotropic as the confining pressure increases. The ratios exponentially decrease as the confining pressure increases, which can be represented by:

$$E/E' = 1.713 \cdot \exp(-0.036\sigma_3) \quad (6.1)$$

where E' and E are the minimum and maximum elastic moduli in direction normal and parallel to the plane of transverse isotropy (bedding plane). The exponential equation fits well to the test results, with R^2 greater than 0.9.

Table 6.1 Results of E/E' ratios.

σ_1 (MPa)	σ_3 (MPa)	E' (GPa)	E (GPa)	E/E'
25.1	0	1.35	2.40	1.78
60.3	5	1.72	2.43	1.41
70.3	8	2.01	2.45	1.22
87.2	15	2.37	2.46	1.04

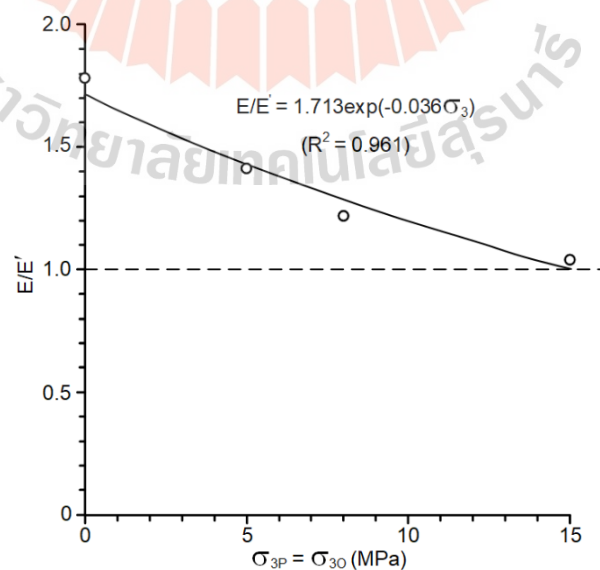


Figure 6.1 Variation of E/E' ratios as a function of confining pressure.

6.3 Transverse isotropic parameters

Applying Amadei's solution to the test results, the apparent elastic modulus (E_y) and Poisson's ratios (ν_{yx} and ν_{yz}) for different bedding plane angles of (β) can be calculated. The normal strains ϵ_x , ϵ_y , ϵ_z and shear strain γ_{xy} can be related to the stress, σ , as follows:

$$\epsilon_x = a_{12}\sigma; \quad \epsilon_y = a_{22}\sigma; \quad \epsilon_z = a_{23}\sigma; \quad \gamma_{xy} = a_{26}\sigma \quad (6.2)$$

where

$$\begin{aligned} a_{12} &= -\frac{\nu'}{E} \sin^4 \beta - \frac{\nu'}{E} \cos^4 \beta + \frac{\sin^2 2\beta}{4} \left(\frac{1}{E} + \frac{1}{E'} - \frac{1}{G'} \right) \\ a_{22} &= \frac{\cos^4 \beta}{E'} + \frac{\sin^4 \beta}{E} + \frac{\sin^2 2\beta}{4} \left(\frac{1}{G'} - \frac{2\nu'}{E'} \right) \\ a_{23} &= -\frac{\nu'}{E} \cos^2 \beta - \frac{\nu}{E} \sin^2 \beta \\ a_{26} &= \sin 2\beta \left[\cos^2 \beta \left(\frac{1}{E'} + \frac{\nu'}{E'} \right) - \sin^2 \beta \left(\frac{1}{E} + \frac{\nu'}{E'} \right) \right] - \frac{\sin 2\beta \cos 2\beta}{2G'} \end{aligned} \quad (6.3)$$

G' is the apparent shear modulus, and ν' is the Poisson's ratio variable. Equations (6.2) and (6.3) can be used to calculate the apparent elastic modulus, E_y , and apparent Poisson's ratios ν_{yx} and ν_{yz} of rock salt, as follows:

$$E_y = \frac{1}{a_{22}}; \quad \nu_{yx} = -\frac{a_{12}}{a_{22}}; \quad \nu_{yz} = -\frac{a_{23}}{a_{22}}. \quad (6.4)$$

Table 6.2 Apparent elastic properties determined on rock salt using uniaxial and triaxial compression test results.

Orientation	$\sigma_{3P} = \sigma_{30}$ (MPa)	E_y (GPa)	ν_{yz}	ν_{yx}
$\beta = 0^\circ$	0	1.35	0.35	0.31
	5	1.72	0.32	0.34
	8	2.01	0.31	0.33
	15	2.37	0.32	0.32
$\beta = 25^\circ$	0	1.43	0.32	0.35
$\beta = 45^\circ$	0	1.64	0.31	0.37
$\beta = 60^\circ$	0	1.93	0.31	0.36
$\beta = 90^\circ$	0	2.40	0.31	0.35
	5	2.43	0.34	0.34
	8	2.45	0.33	0.33
	15	2.46	0.31	0.32

6.3.1 Apparent elastic modulus

The measured elastic modulus varies from 1.35 to 2.46 GPa, depending on the orientations of bedding planes. With larger orientation angles (β) the elastic modulus is higher. Figure 6.2 shows variation of apparent elastic modulus (E_y) under different β angles. The apparent elastic moduli are lower in the direction normal to bedding plane than those parallel to the bedding plane. Under higher confining pressures, the effect of transverse isotropic however tend to decrease.

6.3.2 Apparent Poisson's ratio

The measured Poisson's ratios vary from 0.31 to 0.36, depending on the β angles. They are calculated from the axial and tangential of the stress-strain curves at about 50% of the failure stress. The Poisson's ratios between the directions that are parallel to strike of beds (ν_{yz}) are slightly lower than those between normal to the strike of beds (ν_{yx}). Figure 6.3 shows variation of apparent Poisson's ratio under different β

angles. Dash line is the apparent Poisson's ratio under uniaxial compression test and solid line is the apparent Poisson's ratio with different angles β under confining pressure of 15 MPa. Poisson's ratio tend to be independent of β when the confining pressure increases diagrams in Figures 6.2 and 6.3 suggest that under higher confining pressures both elastic moduli and Poisson's ratios of rock salt tend to be insensitive to the transverse isotropic plane (bedding plane). In other word, the salt tend to behave as an isotropic material under confinement. This may be due to the healing mechanism of the intergranular boundaries of the salt.

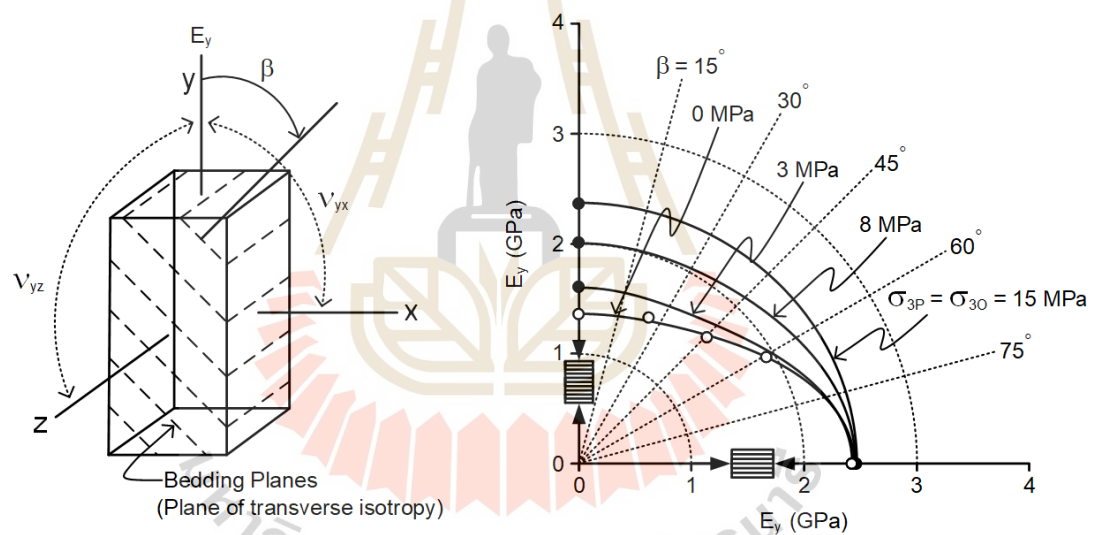


Figure 6.2 Variation of apparent elastic modulus (E_y) under different β angles. Lines are the calculated E_y . Data points are test results

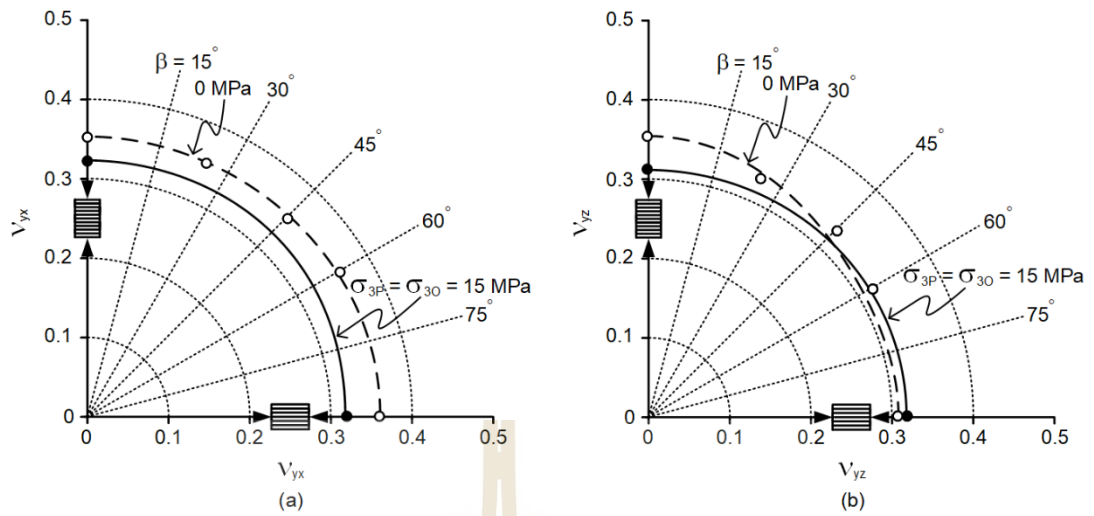


Figure 6.3 Variation of apparent Poisson's ratio v_{yx} (a) and v_{yz} (b) under different β angles. Lines are the calculated apparent Poisson's ratio. Data points are test results.

CHAPTER VII

SALT PILLAR STABILITY ANALYSIS

7.1 Introduction

This chapter presents a potential application of the research findings here to the initial stability analysis of salt pillars in the area where the salt bedding orientations can be varied. Tributary area concept is applied to determine pillar stresses under different depths and extraction ratios.

7.2 Pillar Stress

The tributary area concept is applied to determine the pillar stress (σ_P) and the factor of safety (FS.) for the extraction ratios (e) of 20%, 30%, 40% and 50%. The mine depths are in the range between 200 and 400 m. The stresses on salt pillars can be written as (Hoek and Brown, 1980):

$$\sigma_P = [(\rho H)/(1 - e)] \times 100 \quad (7.1)$$

where ρ is in-situ stress gradient of overburden (approximated here as 0.022 MPa/m), and H is the mine depth. The calculations are made for the depths from 200 to 400 m.

The factor of safety (FS) can be determined as:

$$FS = \sigma_{c(\beta)} / \sigma_P \quad (7.2)$$

where $\sigma_{c(\beta)}$ is the uniaxial compressive strength of salt specimens tested under different

β angles, and σ_P is pillar stress. Figures 7.1 through 7.5 show the factors of safety as a function of pillar stress (σ_P) for different orientation angles. The results suggest that the factor of safety decreases with increasing pillar stresses, as shown in Table 7.1. The factors of safety linearly decrease with increasing of the extraction ratios. Largest factors of safety are obtained for $\beta = 0^\circ$ (bedding planes are in horizontal). The lowest factors of safety are at $\beta = 60^\circ$. This parametric study results can be used to draw a preliminary design of the mine panels where the salt bedding planes are varied.

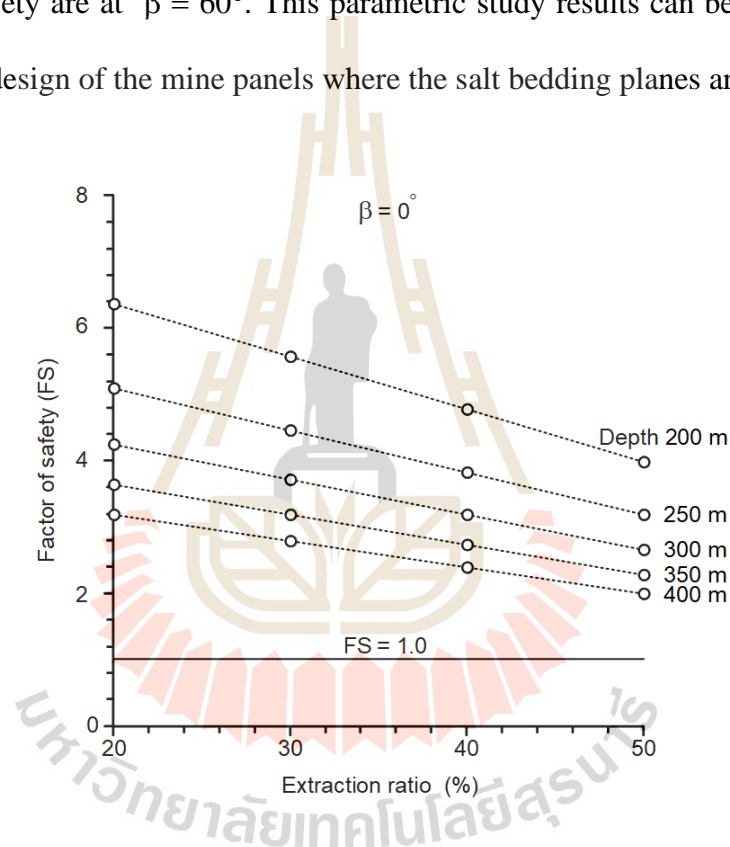


Figure 7.1 Factors of safety as a function of extraction ratio for five mine depths with $\beta = 0^\circ$. Solid line indicate factors of safety equal to 1.

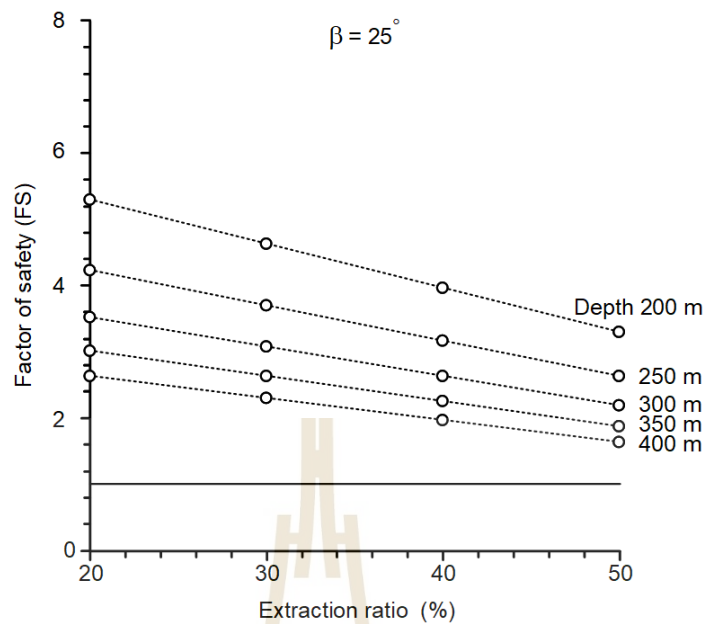


Figure 7.2 Factors of safety as a function of extraction ratio for five mine depths with $\beta = 25^\circ$. Solid line indicate factors of safety equal to 1.

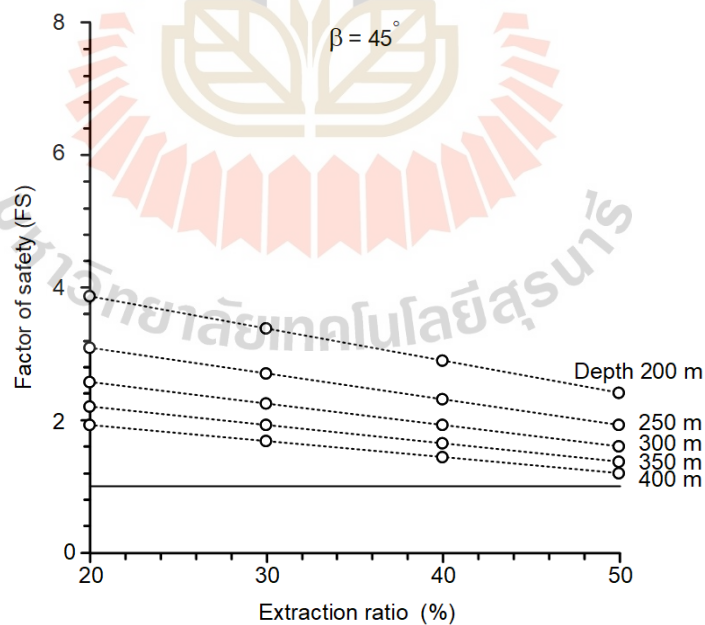


Figure 7.3 Factors of safety as a function of extraction ratio for five mine depths with $\beta = 45^\circ$. Solid line indicate factors of safety equal to 1.

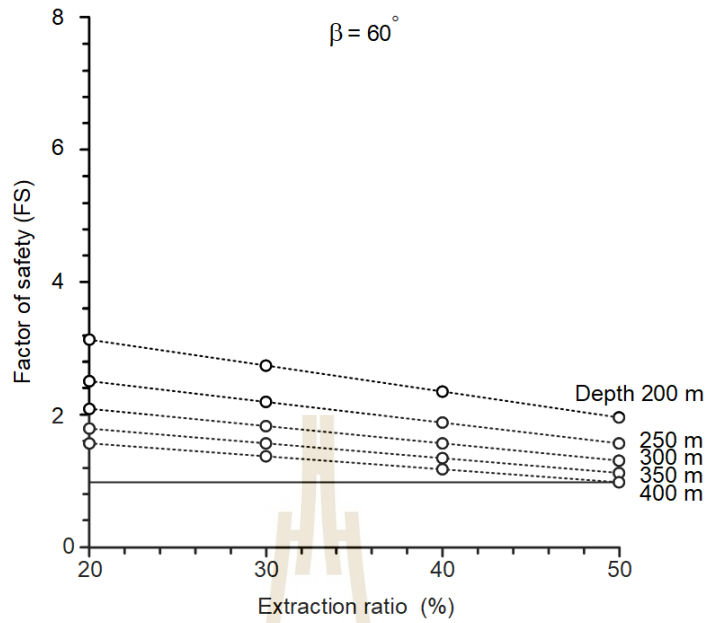


Figure 7.4 Factors of safety as a function of extraction ratio for five mine depths with $\beta = 60^\circ$. Solid line indicate factors of safety equal to 1.

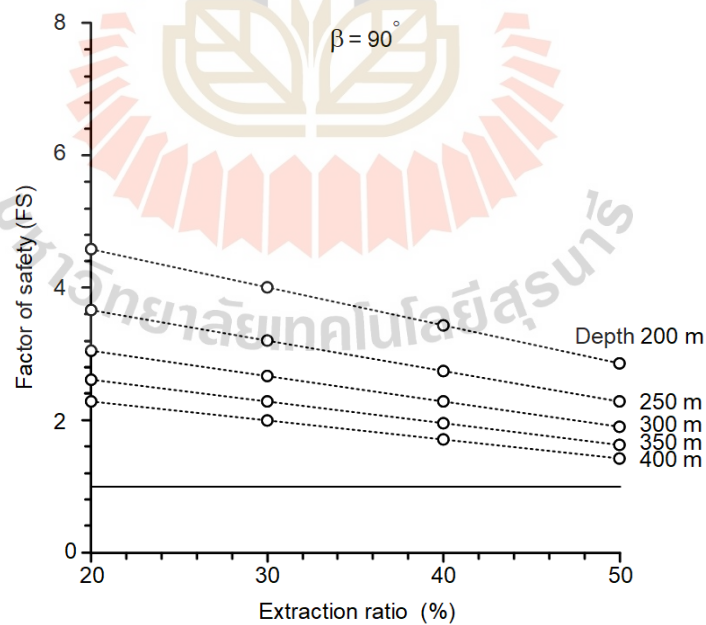


Figure 7.5 Factors of safety as a function of extraction ratio for five mine depths with $\beta = 90^\circ$. Solid line indicate factors of safety equal to 1.

Table 7.1 Depth and factors of safety at different orientation angles.

Depth (m)	Extraction ratio, e (%)	Factors of safety (FS)				
		$\beta = 0^\circ$	$\beta = 25^\circ$	$\beta = 45^\circ$	$\beta = 60^\circ$	$\beta = 90^\circ$
200	20	6.37	5.31	3.88	3.13	4.59
	30	5.57	4.64	3.39	2.74	4.01
	40	4.77	3.98	2.91	2.35	3.44
	50	3.98	3.32	2.42	1.96	2.87
250	20	5.09	4.25	3.10	2.50	3.67
	30	4.46	3.71	2.71	2.19	3.21
	40	3.82	3.18	2.33	1.88	2.75
	50	3.18	2.65	1.94	1.57	2.29
300	20	4.24	3.54	2.58	2.09	3.06
	30	3.71	3.10	2.26	1.83	2.68
	40	3.18	2.65	1.94	1.57	2.29
	50	2.65	2.21	1.62	1.30	1.91
350	20	3.64	3.03	2.22	1.79	2.62
	30	3.18	2.65	1.94	1.57	2.29
	40	2.73	2.27	1.66	1.34	1.97
	50	2.27	1.90	1.38	1.12	1.64
400	20	3.18	2.65	1.94	1.57	2.29
	30	2.79	2.32	1.70	1.37	2.01
	40	2.39	1.99	1.45	1.17	1.72
	50	1.99	1.66	1.21	0.98	1.43

CHAPTER VIII

DISCUSSIONS AND CONCLUSIONS

8.1 Discussions

1) It is found here that the minimum strength of salt occurs when the normal to bedding planes makes an angle (β) of 60 degrees with the loading direction, especially under low confining pressures. This agrees with the test results obtained by McLamore and Gray (1967) on slate and shale, Al-Harhi (1998) and Colak and Unlu (2004) on sandstones, siltstone and claystone, and Saeidi et al. (2013) on sandstone, limestone, shale, slate, gneiss and schist.

2) The effect of transverse isotropy decreases when salt is subjected to higher confining pressures and could reach the isotropic behavior, which is different from the strength envelopes obtained by Jaeger et al. (2007). Colak and Unlu (2004) and Saroglou and Tsiambaos (2008) show that the transversely isotropic effect of most sedimentary rocks remains unchanged even under high confining pressures.

3) The decrease of transversely isotropic effect on rock salt is probably due to that rock salt specimens are capable of self-healing under high confining pressure as suggested by Fuenkajorn and Phueakphum (2011) and Konsaard et al. (2019).

4) The Mohr–Coulomb criterion is applicable under low confining pressures. For a wider range of confinements, Hoek–Brown criterion is more suitable to the test results, as non-linear $\sigma_1 - \sigma_3$ curves are clearly observed, as shown in Figures 5.11 through 5.15.

5) Testing prismatic shaped specimens allows accurate measuring the deformations in the direction parallel and normal to the strike of bedding planes. Such measurement is not possible for cylindrical specimens.

8.2 Conclusions

1) The variation of strength with loading orientations shows U-shaped anisotropy curve where the strength is maximum when loading is perpendicular to the bedding (anisotropic) planes.

2) Hoek and Brown, Coulomb and strain energy criteria can incorporate the effect of transverse isotropy caused by the bedding planes, which can be applied to determine the salt strengths under in-situ conditions. All strength criteria used here give a good estimation of the salt specimen compressive strengths.

3) The Hoek and Brown criterion can well describe the salt strength where the constant m is defined as polynomial function of angle β . The criterion can be useful for the design and stability analysis of support pillars in salt mines where the excavations intersect salt beds that are not in horizontal.

4) The salt strengths increase with increasing confining pressure. The effect of transversely isotropy gradually decreases when the rocks are subjected to higher confining pressures and could reach the isotropic condition. This agrees with the test results obtained by Miller et al. (2013) on mudstone.

5) The measured elastic modulus varies from 1.35 to 2.46 GPa, depending on the orientations of bedding planes. The results show transversely isotropic properties where the elastic modulus in the direction parallel to the bedding planes is greater than that normal to the bedding planes.

6) The measured Poisson's ratios vary from 0.31 to 0.36, depending on the bedding orientations. The Poisson's ratio on the plane parallel to the bedding is lower than those on the plane normal to the bedding.

7) Based on the Amadei solutions, the apparent elastic modulus (E_y) is lower in the direction normal to bedding plane than those parallel to the bedding plane. The apparent Poisson's ratios between the directions that are parallel to strike of bedding plane (ν_{yz}) are slightly lower than those normal to the strike of bedding plane (ν_{yx}). Poisson's ratio tends to be independent of β under high confining pressures.

8) Under higher confining pressures both apparent elastic moduli and Poisson's ratios of rock salt tend to be insensitive to the transverse isotropic plane (bedding plane). In other word, the salt tend to behave as an isotropic material under confinement. This may be due to the healing mechanism of the intergranular boundaries of the salt.

8.3 Recommendations for future studies

The uncertainties of the investigation and results discussed above lead to the recommendations for further studies as follows.

1. Increasing the number of the specimens would statistically enhance the predictability of the test results and the reliability of the proposed strength criteria.
2. Mathematical relation between elastic moduli, Poisson's ratio and bedding orientations under confinement is highly desirable.
3. Testing of rock salt under confining pressures greater than those used here would confirm the postulation that the bedded salt could become isotropic under very high confinement.

REFERENCES

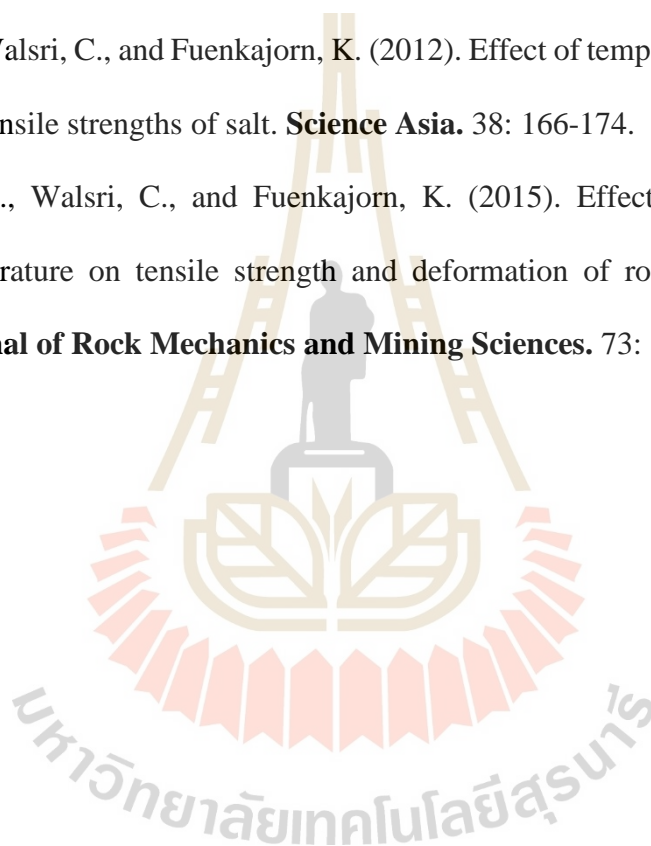
- Al-Ajmi, A.M. and Zimmerman, R.W. (2005). Relation between the Mogi and the Coulomb failure criteria. **International Journal of Rock Mechanics and Mining Sciences**. 42: 431-439.
- Al-Harhi, A. A. (1998). Effect of planar structures on the anisotropy of Ranyah sandstone, Saudi Arabia. **Engineering geology**. 50(1-2): 49-57.
- Amadei, B. (1996). Importance of anisotropy when estimating and measuring in situ stresses in rock. **International Journal of Rock Mechanics and Mining Sciences & Geomechanics Abstracts**. 33(3): 293-325.
- Amadei, B., Savage, W. Z., and Swolfs, H. S. (1987). Gravitational stresses in anisotropic rock masses. **International Journal of Rock Mechanics and Mining Sciences & Geomechanics Abstracts**. 24: 5-14.
- Archeeploha, S., Khamrat, S., and Fuenkajorn, K. (2017). Effects of intermediate principal stress on creep closure of storage caverns in Maha Sarakham salt. **Songklanakarin Journal of Science and Technology**. 39(2): 143-151.
- Artkhonghan, K., Sartkaew, S., Thongrapha, T., and Fuenkajorn, K. (2018). Effects of stress path on shear strength of a rock salt. **International Journal of Rock Mechanics and Mining Sciences**. 104: 78-83.
- ASTM D7012-14 (2014). **Standard Test Methods for Compressive Strength and Elastic Moduli of Intact Rock Core Specimens under Varying States of Stress and Temperatures**, ASTM International, West Conshohocken, PA.

- Batugin, S. A. and Nirenburg, R. K. (1972). Approximate relation between the elastic constants of anisotropic rocks and the anisotropy parameters. **Soviet Mining**. 8(1): 5-9.
- Cho, J. W., Kim, H., Jeon, S., and Min, K. B. (2012). Deformation and strength anisotropy of Asan gneiss, Boryeong shale, and Yeoncheon schist. **International Journal of Rock Mechanics and Mining Sciences**. 50: 158-169.
- Chobsranoi, M. and Fuenkajorn, K. (2016). Maximum unsupported span and standup time of potash mine roof as affected by carnallite contents. In **Proceedings of the 9th Asian Rock Mechanics Symposium**. 18-20 October 2016, Bali, Indonesia.
- Colak, K. and Unlu, T. (2004). Effect of transverse anisotropy on the Hoek-Brown strength parameter 'mi' for intact rocks. **International Journal of Rock Mechanics and Mining Sciences**. 41(6): 1045-1052.
- Fuenkajorn, K. and Phueakphum, D. (2011). Laboratory assessment of healing of fractures in rock salt. **Bulletin of Engineering Geology and the Environment**. 70(4): 665.
- Fuenkajorn, K., Sriapai, T., and Samsri, P. (2012). Effects of loading rate on strength and deformability of Maha Sarakham salt. **Engineering Geology**. 135-136: 10-23.
- Fuenkajorn, K., Walsri, C., and Phueakphum, D. (2011). Intrinsic variability of the mechanical properties of Maha Sarakham salt. **Quarterly Journal of Engineering Geology and Hydrogeology**. 44: 445-456.

- Gerrard, C. M. (1975). Background to mathematical modelling in geomechanics-the roles of fabric and stress history. In **Finite Elements in Geomechanics**. pp. 33-120. John Wiley & Sons. United Kingdom.
- Goshtasbi, K., Ahmadi, M., and Seyedi, J. (2006). Anisotropic strength behaviour of slates in the Sirjan-Sanandaj zone. **Journal-South African Institute of Mining and Metallurgy**. 106(1): 71-75.
- Hakala, M., Kuula, H., and Hudson, J. A. (2007). Estimating the transversely isotropic elastic intact rock properties for in situ stress measurement data reduction: A case study of the Olkiluoto mica gneiss, Finland. **International Journal of Rock Mechanics and Mining Sciences**. 44(1): 14-46.
- Hoek, E. and Brown, E.T. (1980). Empirical strength criterion for rock masses. **Journal of Geotechnical Engineering ASCE**. 160(GT9): 1013-1035.
- Hu, S. C., Tan, Y. L., Zhou, H., Guo, W. Y., Hu, D. W., Meng, F. Z., and Liu, Z. G. (2017). Impact of bedding planes on mechanical properties of sandstone. **Rock Mechanics and Rock Engineering**. 50(8): 2243-2251.
- Jaeger, J.C., Cook, N.G.W., and Zimmerman, R.W. (2007). **Fundamentals of Rock Mechanics**. Blackweel: Oxford. 475p.
- Junthong, P., Khamrat, S., Sartkaew, S., and Fuenkajorn, K. (2019). Determination of time-dependent strengths of salt pillars based on strain energy principle. **International Journal of Mining Science and Technology**. 29(2): 273-279.
- Konsaard, K., Khamrat, S., Thongrapha, T., and Phueakphum, D. (2019). Healing effectiveness of fractures in rock salt and potash. **Engineering Journal of Research and Development**. 30(1): 113-122.

- Liao, J.J. and Hsieh, H.Y. (1999). Triaxial residual strength of an anisotropic rock. **Rock Mechanics for Industry**. pp. 317-324.
- Luangthip, A., Wilalak, N., Thongprapha, T., and Fuenkajorn, K. (2017). Effects of carnallite content on mechanical properties of Maha Sarakham rock salt. **Arabian Journal of Geosciences**. vol. 10(6).
- McLamore, R. and Gray, K.E. (1967). The mechanical behavior of anisotropic sedimentary rocks. **Journal of Manufacturing Science and Engineering**. 89(1): 62-73.
- Miller, D., Plumb, R., and Boitnott, G. (2013). Compressive strength and elastic properties of a transversely isotropic calcareous mudstone. **Geophysical Prospecting**. 61: 315-328.
- Nasseri, M.H.B., Rao, K.S., and Ramamurthy, T. (2002) Anisotropic strength and deformational behavior of Himalayan schists. **International Journal of Rock Mechanics and Mining Sciences**. 40(1): 3-23.
- Phatthaisong, K., Suratwadee, S., and Kittitep, F. (2018). Effects of loading rate and temperature on strength and deformability of Maha Sarakham salt. **Songklanakarin Journal of Science and Technology**. 40(2): 359-366.
- Ramamurthy, T. (1993). **Strength and Modulus Responses of Anisotropic Rocks**. Pergamon, Oxford.
- Saeidi, O., Vaneghi, R. G., Rasouli, V., and Gholami, R. (2013). A modified empirical criterion for strength of transversely anisotropic rocks with metamorphic origin. **Bulletin of Engineering Geology and the Environment**. 72(2): 257-269.

- Samsri, P., Sriapai, T., Walsri, C., and Fuenkajorn, K. (2010). Polyaxial creep testing of rock salt. In **Proceedings of the 3th Thailand Symposium on Rock Mechanics** (pp. 125-132). Thailand.
- Saroglou, H. and Tsiambaos, G. (2008). A modified Hoek–Brown failure criterion for anisotropic intact rock. **International Journal of Rock Mechanics and Mining Sciences**. 45(2): 223-234.
- Sriapai, T., Walsri, C., and Fuenkajorn, K. (2012). Effect of temperature on compressive and tensile strengths of salt. **Science Asia**. 38: 166-174.
- Wisetsaen, S., Walsri, C., and Fuenkajorn, K. (2015). Effects of loading rate and temperature on tensile strength and deformation of rock salt. **International Journal of Rock Mechanics and Mining Sciences**. 73: 10-14.



BIOGRAPHY

Mr. Nattapon Sukjaroen was born on August 18, 1995 in Bangkok, Thailand. He received his Bachelor's Degree in Engineering (Geological Engineering) from Suranaree University of Technology in 2018. For his post-graduate, he continued to study with a Master's degree in the Geological Engineering Program, Institute of Engineering, Suranaree university of Technology. During graduation, 2018-2020, he was a part time worker in position of research assistant at the Geomechanics Research Unit, Institute of Engineering, Suranaree University of Technology.

